[American Journal of Science, Vol. 318, December, 2018, P. 989–1017, DOI 10.2475/10.2018.01]

American Journal of Science

DECEMBER 2018

COUPLED PRECAMBRIAN CRUSTAL EVOLUTION AND SUPERCONTINENT CYCLES: INSIGHTS FROM *IN-SITU* U-Pb, O- AND Hf-ISOTOPES IN DETRITAL ZIRCON, NW INDIA

WEI WANG*,**,†, PETER A. CAWOOD**, MANOJ K. PANDIT***, XIAO-PING XIA§, and JUN-HONG ZHAO*

ABSTRACT. Oxygen and hafnium isotopic compositions, measured *in-situ* on U-Pb dated zircon grains from Paleoproterozoic to early Cambrian successions in NW India have implication for regional crustal evolution and supercontinent cycles. Analyzed zircon grains have high Th/U ratios (>0.1), display strongly fractionated REE patterns, metamorphic overprint, and evidence of interaction with low temperature fluids. Their positive Ce and negative Eu anomalies preclude any Pb loss after zircon crystallization. The U-Pb age spectra (concordance between 90 and 110%) indicate prominent peaks at 2.6 to 2.4 Ga, 1.9 to 1.7 Ga, 1.6 to 1.5 Ga, 1.2 to 1.0 Ga and 0.9 to 0.7 Ga that coincide with the assembly and breakup of Precambrian supercontinents. The Hf model ages of zircon grains with mantle like $\delta^{18}O$ values reveal continuous generation of the continental crust from 3.3 to 1.3 Ga in NW India with major episodes during 3.3 to 2.7 Ga and 1.7 to 1.5 Ga. These ages correspond well with the 3.4 to 2.9 Ga and 2.2 to 1.6 Ga age peaks recognized in detrital zircon populations from eastern Australia and North America, underlining the significance of these time brackets in continental crust generation during the global continental evolution. Magmatic episodes at 1.9 to 1.7, 1.2 to 1.0 and 0.9 to 0.7 Ga are considered to represent crustal reworking rather than juvenile addition and the former two phases correspond with periods of supercontinent assembly. However, a progressive depletion in ^{18}O from supra-mantle to mantle values in the 1.7 to 1.5 Ga zircons, coupled with their mantle-like $\varepsilon_{Hf(t)}$ values, indicate at least some juvenile input. Moreover, the 1344 to 1120 Ma zircon grains with low $\delta^{18}O$ (3.7–1.5‰) but high $\varepsilon_{Hf(t)}$ (+8.1− +1.9 with one exception of −2.5) values signify rapid reworking of mantle derived materials in an extensional setting during this period. The 0.9 to 0.7 Ga peak, corresponding to the fragmentation of Rodinia supercontinent, documents crustal reworking that is in contradiction to the generally considered juvenile crustal addition in extensional setting associated with supercontinent breakup.

Keywords: U-Pb-Hf-O-isotopes, detrital zircon ages, NW India, crustal evolution, Supercontinent cycles

INTRODUCTION

The evolution of, and interactions between, Earth's atmosphere, hydrosphere, lithosphere and mantle are documented in the preserved rock record (Cawood and others, 2013a). However, timing of continental crust generation and its evolutionary history are not yet fully understood, resulting in first order uncertainties, both in the

* State Key Laboratory of Geological Processes and Mineral Resources, School of Earth Sciences, China University of Geosciences, Wuhan 430074, China
** School of Earth, Atmosphere & Environment, Monash University, Melbourne, Victoria 3800, Australia
*** Department of Geology, University of Rajasthan, Jaipur 302004, Rajasthan, India
§ Guangzhou Institute of Geochemistry, Chinese Academy of Sciences, Guangzhou, China
† Corresponding Author: Wei Wang, wwz@cug.edu.cn

mechanism and extent of interactions, especially for the early Earth (Hawkesworth and others, 2017). Secular variations in generation and reworking of continental crust are known to be influenced by the supercontinent cycles (Campbell and Allen, 2008; Hawkesworth and others, 2009; Nance and others, 2014). Whether the balance between generation and destruction of continental crust during different supercontinent cycles is uniformly recorded in different continents, independent of their paleoposition in supercontinent configurations (Roberts and Slagstad, 2015) or selectively recorded (Spencer and others, 2013), remains controversial.

Zircon has become a major tool in modeling crustal evolution due to its resistance to physico-chemical alteration during multiple cycles of sedimentation and low to medium grade metamorphism, and the ability to measure multiple isotopic systems and trace element compositions within an individual grain or part there of (Hawkesworth and others, 2010; Wang and others, 2011; Cawood and others, 2013a; Spencer and others, 2017). Zircon U-Pb ages, in concert with *in-situ* Lu-Hf and O-isotopic characteristics, can provide a record of crust generation events and preservation, thus enabling 'fingerprinting' and reconstruction of tectonic histories of crustal segments (Hawkesworth and Kemp, 2006; Kemp and others, 2006; Wang and others, 2009; Iizuka and others, 2013; Wang and others, 2013; Wan and others, 2015).

Zircons from well-preserved Proterozoic (Paleo- to Neoproterozoic) supracrustals in Peninsular India, overlying an Archean tonalite-trondhjemite-granodiorite (TTG) basement, can be used for modeling Precambrian crustal evolution of this crustal segment. Studies based on limited detrital zircon U-Pb and Hf-isotopic data have identified episodic juvenile crustal additions at 3.2 Ga, 2.9 Ga, 2.7 Ga, 2.5 Ga, and 1.87 to 1.80 Ga in NW India (Condie and others, 2005; Kaur and others, 2011, 2013). However, zircon U-Pb ages and Lu-Hf isotopic characteristics are incapable of fingerprinting hybrid or real crust-mantle differentiation time. For a better resolution of crustal growth history of NW India, we carried out U-Pb, Lu-Hf and O- isotopic analyses of detrital zircons from five metasedimentary rock units representing Paleoproterozoic to early Cambrian successions. The data have been interpreted in terms of discrimination of crust generation events, reworking and growth and their relationship to the contemporary supercontinent cycles.

GEOLOGICAL BACKGROUND AND SAMPLING

Peninsular India is a collage of five Archean cratonic nuclei; the Banded Gneiss Complex (BGC in Aravalli Mountain Region in NW India), Bundelkhand, Singhbhum, Bastar and Dharwar cratons, thought to have stabilized during the late Archean (Meert and Pandit, 2015 and references therein). The Aravalli-BGC constitutes a Paleo- to Neoarchean cratonic nucleus (~3.3–2.5 Ga) with predominant TTG gneisses and granitoids along with minor metavolanic rocks, mafic intrusions and metasedimentary components (Wiedenbeck and Goswami, 1994; Roy and Kröner, 1996; Sinha Roy and others, 1998) (figs. 1 and 2A). This basement complex is overlain by two Proterozoic supracrustal successions, namely the Aravalli and Delhi supergroups, together constituting the >750 km long, NE - SW trending Aravalli-Delhi fold belt in Aravalli Mountain Region in NW India. This belt, together with the BGC, is separated from the Bundelkhand Craton by the Great Boundary Fault to the east and from the Bastar and Singhbhum cratons by the Central India Tectonic zone to the south.

The Aravalli Supergroup is the older cover succession, unconformably deposited over an Archean (BGC) basement. The Aravalli rocks are exposed in the southeastern part of the Aravalli-Delhi Belt (fig. 1) showing best development around the type area in the Udaipur valley (fig. 2B). Depositional age of Aravalli sedimentary rocks is not clearly defined due to the lack of suitable datable material and is loosely constrained between ~2.5 Ga (age of basement granites; Wiedenbeck and others, 1996) and ~1.6 Ga (age of the youngest detrital zircons; McKenzie and others, 2013; Wang and others,

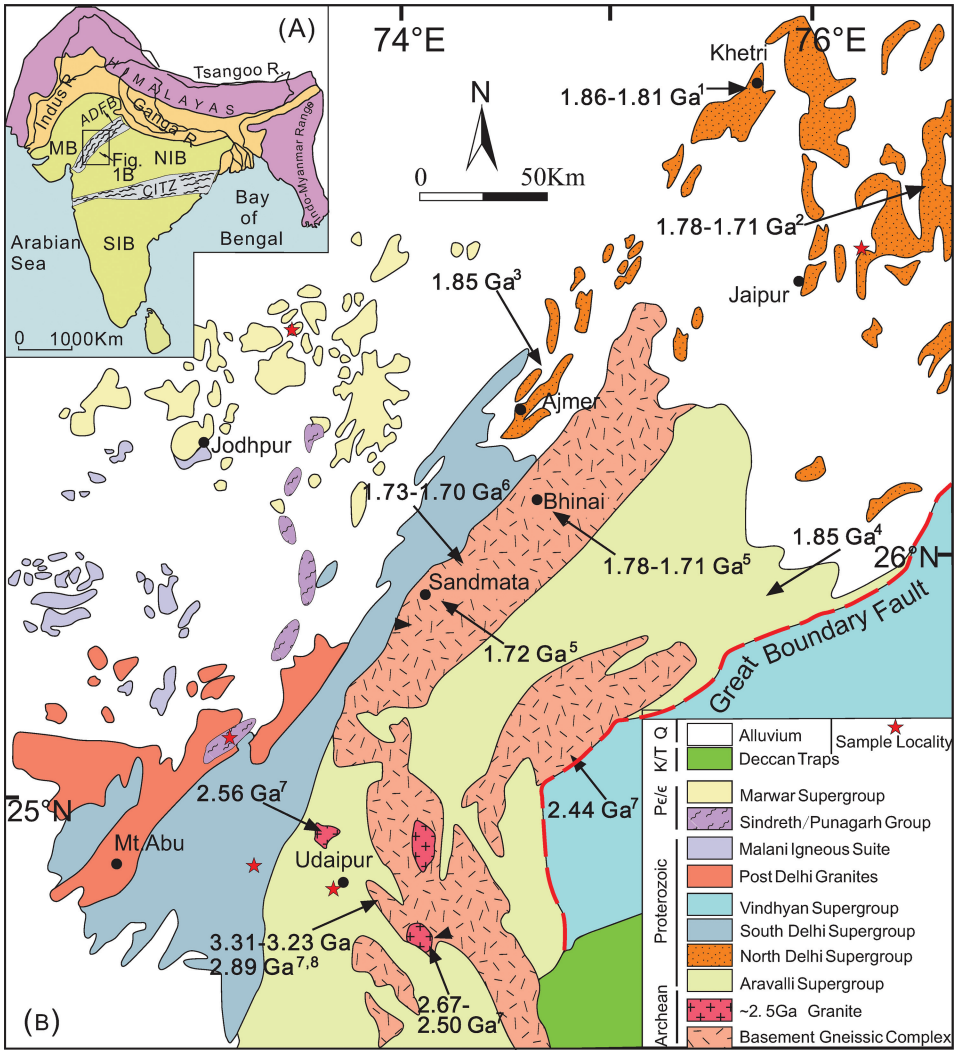

Fig. 1. (A) Framework of Peninsular India (after Roy and Jakhar, 2002); (B) Simplified geological map showing distribution of major Precambrian geological units of the Aravalli-Delhi Belt (adapted from Roy and Jakhar, 2002; Meert and Pandit, 2015; Wang and others, 2019). Age data source, (1) (Kaur and others, 2009, 2011, 2017b); (2) (Biju-Sekhar and others, 2003; Kaur and others, 2017a); (3) (Mukhopadhyay and others, 2000); (4) (Deb and others, 2002); (5) (Buick and others, 2006); (6) (Bhowmik and others, 2010); (7) (Wiedenbeck and others, 1996; Roy and Kröner, 1996); (8) (Gopalan and others, 1990). Abbreviations: ADFB-Aravalli Delhi Fold Belt, CITZ-Central Indian Tectonic Zone, MB-Marwar Block, NIB-North Indian Block, SIB-South Indian Block.

2019). Detailed study has suggested that the rocks of the Aravalli Supergroup archive the record for the development of an early Paleoproterozoic passive-margin platform, followed by transition to continental arc and subsequently to an evolved rift basin-passive margin setting (Wang and others, 2019). Delhi Supergroup rocks display a diachronous depositional history and variation in the degree of deformation (figs. 2C and 2D), and are divided into an older North Delhi Group (~1.7 Ga) and a younger (>1.0 Ga) South Delhi Group (Kaur and others, 2011, 2013, 2017a; McKenzie and others, 2013; Wang and others, 2017a). The South Delhi Group has a tectonized

Fig. 2. Photographs showing outcrop features of TTG basement and overlying sedimentary sequences. (A) Typical TTG gneiss of the BGC-I, to the south of Udaipur city; (B) wavy bedding of the Udaipur sandstone, middle Aravalli Supergroup; (C) straight ripple marks in the Alwar Group quartzite, Northern Delhi Supergroup, showing truncation at right angles by sinuous ripple marks; (D) recumbent folding in strongly deformed quartzite of the Kumbhalgarh Group, Southern Delhi Supergroup; (E) quartz sandstone and gavel-bearing sandstone of the Nargaur Group, upper Marwar Supergroup; (F) upright fold in the arkose at Argo Dam, Sindreth Group.

contact with Aravalli Group rocks (Heron, 1953; Sinha Roy and others, 1998; Roy and Jakhar, 2002) however, both northern and southern Delhi groups unconformably overlie Archean basement (Sinha Roy and others, 1998; Roy and Jakhar, 2002). Neoproterozoic events in the NW Indian block begun with the ~1.0 Ga eastward convergence and subsequent collision of the Marwar Block in the west and the Aravalli - Delhi Belt in the east, resulting in emplacement of 968 ±1 Ma calc-alkaline granitoids

and associated mafic intrusions, and 990 ± 6 Ma and 987 ± 6.4 Ma rhyolites in the Sendra – Ambaji arc terrane along the western margin of the Aravalli-Delhi fold belt (Deb and others, 2001; Pandit and others, 2003). Several granitoid intrusions occurred in the southern Delhi Fold Belt during 870 to 800 Ma, collectively designated as the Erinpura Granite (Heron, 1953; Deb and others, 2001; Just and others, 2011; Solanki, ms, 2011; Zhao and others, 2018). A younger, more extensive, largely subaerial magmatic event, comprising visibly undeformed and unmetamorphosed felsic (predominantly) rocks in the region further west, is termed the Malani Igneous Suite (MIS; Pareek, 1981). Multiple episodes of MIS magmatism have been dated to 780 to 750 Ma with some minor ultrapotassic rhyolite at 680 Ma (Rathore and others, 1999; Torsvik and others, 2001b; Gregory and others, 2009; Meert and others, 2013; Wang and others, 2017b, 2019; de Wall and others, 2018). More recent studies have included bimodal volcaniclastic sequences in the linear Sindreth and Punagarh basins (Van Lente and others, 2009; Dharma Rao and others, 2012; Wang and others, 2018) and variably deformed Mt. Abu granitoids (de Wall and others, 2012; Ashwal and others, 2013) and similar rocks of Nagar Parkar in SE Pakistan (de Wall and others, 2018; Jan and others, 2018) in the ambit of MIS. Unconformably overlying the Malani Igneous Suite is the Marwar Supergroup, a late Neoproterozoic to Early Cambrian undeformed sedimentary sequence (Pareek, 1984; Pandit and others 2001) deposited in a NNE-SSW trending basin, attaining a cumulative thickness of over 2000 m (Pareek, 1984). The Marwar Supergroup is subdivided (from oldest to youngest) into the Jodhpur (arenaceous), Bilara (carbonate) and Nagaur (argillaceous/arenaceous) groups.

ANALYTICAL METHODS

For the present study five (meta)sandstone and conglomerate samples representing different stratigraphic units from Paleoproterozoic Aravalli Supergroup to Late Neoproterozoic-Early Cambrian Marwar Supergroup were analyzed for isotopic studies. Details of analytical methods are discussed in the following sections.

Approximately 2 kg each of fresh sample was processed for zircon separation using standard density and magnetic separation techniques and handpicking under binocular microscope. The separated zircon grains, together with zircon standards Pelsovice and Penglai, were mounted in epoxy resin and polished to expose the center of the grains. Morphology and internal structure of zircon were determined using a Gatan Mono CL 4+ attached to Carl Zeiss SUPRA55SAPPHIR, housed at the Guangzhou Institute of Geochemistry, Chinese Academy of Science. Cathodoluminescence (CL) images were used to select grains suitable for *in-situ* analyses, avoiding inherited cores, inclusions and fractures. During the *in-situ* analyses of U-Pb, Lu-Hf and O isotopes, zircon grains were selected randomly, regardless of their morphology and grain size.

In-situ zircon oxygen isotopes were determined using the Cameca IMS-1280 SIMS housed at Guangzhou Institute of Geochemistry, Chinese Academy of Science. The primary $^{133}Cs+$ ion beam with an intensity of ~2 nA was accelerated at 10 kV to bombard the grain surface. The spot size was about 20 μm in diameter, including ~10 μm area focused by Gaussian mode and rastered over a 10 μm area. The normal incidence electron flood gun was used to compensate for sample charging. Negative secondary ions were extracted with a −10 kV potential. Oxygen isotopes were determined using a multi-collection mode on two off-axis Faraday cups and the mass resolution used to measure oxygen isotopes was *ca.* 2500. Total analytical time for each spot was about 3.5 minutes, including 30 s of pre-sputtering, 120 s of automatic tuning of the secondary beam, and 64 s of analysis. Measured $^{18}O/^{16}O$ ratios were normalized to Vienna Standard Mean Ocean Water compositions (VSMOW; $^{18}O/^{16}O = 0.0020052$), and then corrected for instrumental mass fractionation (IMF) using the Penglai zircon standard [($\delta^{18}O_{VSMOW} = 5.3‰$ (Li and others, 2010)], which was analyzed once every four unknowns, using sample-standard bracketing (SSB) method. The internal preci-

sion of each analysis generally was better than 0.1 permil (1σ) for the $^{18}O/^{16}O$ ratio. As discussed in Valley and Kita (2009), internal precision for a single spot (commonly <0.1‰, 1σ) is not a good index of analytical quality for stable isotope ratios measured by SIMS. Therefore, the external precision, measured by the spot-to-spot reproducibility of repeated analyses of the Penglai standard, 0.32 permil (2SD, n = 41) was adopted for data evaluation. Measurements of the Qinghu zircon standard as an unknown sample during the course of this study yielded a weighted mean of $\delta^{18}O = 5.47‰ \pm 0.11‰$ (2SD), which is consistent, within error, with the reported value of 5.4‰ ± 0.2‰ (Li and others, 2013). Detailed analytical methods are described in Li and others (2010) and Yang and others (2018).

In situ zircon U-Pb isotope measurements were carried out using an Agilent 7500a ICPMS coupled to a 193 nm ArF Excimer Laser ablation system (GeoLas 2005, Lambda Physik) housed at State Key Laboratory of Geological Processes and Mineral Resources (SKLGPM), China University of Geosciences, Wuhan. Abundances of Ti, Y, Nb, REEs, Hf, Ta and Th were also determined concurrently with the U-Pb isotopic dating. The ArF Excimer laser was initially homogenized by a set of beam delivery systems and then focused on the zircon surface with the fluence of $10 J/cm^2$. A spot diameter of 32 μm with 5 Hz repetition rate was employed for 45 seconds as the ablation protocol. Helium was used as a carrier gas to provide efficient aerosol transport to the ICP and to minimize aerosol deposition around the ablation site and within the transport tube. The carrier and make-up gas flows were optimized by monitoring ^{238}U intensity during ablating NIST610. In order to enhance the sensitivity of U, Th, and Pb isotopes, 2 to 4 mL/min of nitrogen was added to the central gas flow. A novel "wire" signal smoothing device was applied to improve the signal stability. Ratios and absolute abundances of U-Pb isotopes were measured relative to the 91500 zircon standard, while zircon standard GJ-1 was analyzed as unknown sample for quality control. Trace element compositions of zircons were externally calibrated against NIST SRM 610 with ^{91}Zr as the secondary standard. Raw data reduction was performed off-line by *ICPMSDataCal* (Liu and others, 2010a) and the results are reported with 2σ errors level. Common Pb correction was applied following the method of Andersen (2002) and the difference between common Pb corrected and uncorrected ages was generally small. Data were processed using the program ISOPLOT (Ludwig, 2003). Mean ages for pooled U/Pb (and Pb/Pb) analyses are quoted with 95 percent confidence. Detailed metadata related to the laboratory and sample preparation methods are summarized in table S1 (http://earth.geology.yale.edu/%7eajs/SupplementaryData/2018/Wang). The obtained mean $^{206}Pb/^{238}U$ ages for reference materials GJ-1is 600.5±1.8 Ma (2σ, MSWD = 0.6, n = 25) are consistent with the recommended value of 599.8 ± 1.7 Ma(2σ) by Jackson and others (2004).

The zircon grains analyzed for U-Pb and O isotopes were also selected for *in-situ* Lu-Hf isotopic analyses by Neptune Plus multi-collector (MC)-ICPMS, coupled to a GeoLas2005 laser ablation system in SKLGPM. The Hf isotopes were analyzed with a beam diameter of 44 μm, pulse rate of 10 Hz and energy density of $4 J/cm^2$. Helium was used as the carrier gas within the ablation cell and was merged with argon (makeup gas) after the ablation cell to enhance the signal intensity. Atomic masses 171 to 182 were simultaneously measured in a static-collection mode. The real time mass fractionation of Yb (β_{Yb}) was directly obtained from the zircon sample itself. Instrumental mass bias correction of Yb isotope ratios were normalized to $^{173}Yb/^{171}Yb$ of 1.35274 (Thirlwall and Anczkiewicz, 2004) and $^{176}Hf/^{177}Hf$ ratios to $^{179}Hf/^{177}Hf$ of 0.7325 (Patchett and Tatsumoto, 1981) using an exponential law. Interference of ^{176}Yb on ^{176}Hf was corrected by measuring the interference-free ^{173}Yb isotope, using $^{176}Yb/^{173}Yb = 0.78696$ (Thirlwall and Anczkiewicz, 2004) to calculate $^{176}Yb/^{177}Hf$. Similarly, the relatively minor interference of ^{176}Lu on ^{176}Hf was corrected by measuring the

intensity of the interference-free ^{175}Lu isotope and using the recommended $^{176}Lu/^{175}Lu = 0.02656$ (Blichert-Toft and others, 1997) to calculate $^{176}Lu/^{177}Hf$. The mass bias of Yb (β_{Yb}) was used to calculate the mass fractionation of Lu. Detailed procedures are described in Liu and others (2010b). Zircon standards 91500 and GJ-1 were measured along with unknown samples to ensure reliability of the analytical data. The Hf model ages were calculated back to the time of juvenile continental crust with average $\varepsilon_{Hf} = +13.0$ (Iizuka and others, 2013), assuming that zircons crystallized from magmas with Hf ratios similar to that of the bulk Precambrian continental crust (0.093: Vervoort and Patchett, 1996). Detailed metadata related to the laboratory and sample preparation methods are summarized in table S1 (http://earth.geology.yale.edu/%7eajs/SupplementaryData/2018/Wang).

RESULTS

Zircon U-Pb, Hf- and O-isotopic data are presented in table 1 and detailed isotopic compositions are shown in supplementary tables (http://earth.geology.yale.edu/%7eajs/SupplementaryData/2018/Wang).

U-Pb Ages

Representative Cl images of studied zircons are displayed in figure 3. All zircon grains show variable degrees of rounding, with oscillatory zoning observed in most grains (fig. 3). The U-Pb isotopic compositions are presented in table S2 (http://earth.geology.yale.edu/%7eajs/SupplementaryData/2018/Wang) and illustrated as Concordia diagrams (figs. 4A-4E) and histograms of U-Pb concordant age populations (figs. 4F–4J, with 90–110% concordance). Only the concordant U-Pb ages have been used for further discussion and interpretation, unless otherwise specified.

Zircons from Aravalli Supergroup (DLW1450) and northern Delhi Group (DLW1412) show similar age distribution with a prominent age peak at 1.85 to 1.65 Ga and a smaller one at ~2.5 Ga (figs. 4F and 4G). Zircons from sample DLW1473, from the southern Delhi Supergroup, define 1.7 to 1.4 and 1.3 to 1.0 Ga age groupings (fig. 4H). Samples from the Sindreth Group (RJW1427) of the Malani Igneous Suite and the Nagaur Group of the Marwar Supergroup (RJW14104) display similar zircon age distributions, defined by a prominent age group at 0.9 to 0.7 Ga and minor broad peaks at ~2.5 and 2.0 to 1.5 Ga (figs. 4I and 4J). The Neoproterozoic age peak in sample RJW14104 (~790 Ma) is slightly younger than that of RJW1427 (~870 Ma). Two zircon grains with $^{207}Pb/^{206}Pb$ ages of 3400±24 Ma (DLW1450-31) and 3257 ±24 Ma (DLW143-64) represent the only two Paleoarchean ages in the analyzed samples.

Trace element data for zircons are presented in table S3 (http://earth.geology.yale.edu/%7eajs/SupplementaryData/2018/Wang) and plotted against U-Pb ages in figure 5. Most zircon grains have ΣREE between 300 and 3000 ppm (table S3, fig. 5A), similar to the values observed in zircons hosted in granite and significantly higher than zircon from carbonatite and kimberlite (Hoskin and Schaltegger, 2003). All the zircon grains show a wide range of trace element abundances, however, with similar patterns in binary plots against U-Pb age (fig. 5B), except the stronger negative anomalies of Eu observed since ~2.0 Ga. Nearly all the zircon grains exhibit similar REE patterns, characterized by negative Eu and positive Ce anomalies, and prominent enrichment of HREE over LREE and MREE, a feature typical of continental crustal zircons (Hoskin and Ireland, 2000; Wu and Zheng, 2004) (figs. 5C and 5D). All the zircons have Th/U ratios greater than 0.1 (majority with >0.2), typical of magmatic zircons (fig. 5E; Hoskin and Ireland, 2000).

Lu-Hf Isotopes

In-situ Lu-Hf isotopic data are summarized in table S4 (http://earth.geology.yale.edu/%7eajs/SupplementaryData/2018/Wang) and plotted against their crystalli-

TABLE 1

Synthesis of U-Pb-Hf-O isotopes for detrital zircons from NW India

Sample No.	$\delta^{18}O$		εHf(t)		$T_{(DM2)}$[a]	±s	$T_{(DM)\ AC}$[b]		$\Delta\varepsilon Hf_{AM}$[c]	U-Pb ages[d]	
	‰	±s		±s	Ga		Ga	±s	ε	Ma	1σ
Sample DLW1450, a sandstone from the Aravalli Supergroup, N.24°33'05.2", E.73°41'13.0"											
DLW1450-01	5.96	0.06	-3.3	0.4	2.62	0.02	2.37	0.02	-12.2	1742	33
DLW1450-02	8.23	0.08	0.4	0.5	2.41	0.02	2.20	0.02	-8.5	1762	46
DLW1450-03	5.67	0.08	0.6	0.6	2.60	0.02	2.41	0.02	-7.5	2021	44
DLW1450-04	8.77	0.06	0.3	0.6	2.42	0.02	2.21	0.02	-8.5	1773	30
DLW1450-05	8.97	0.09	-2.2	0.4	2.55	0.02	2.32	0.02	-11.1	1744	30
DLW1450-06	8.87	0.11	-1.4	0.6	2.53	0.02	2.30	0.02	-10.3	1770	34
DLW1450-07	7.61	0.11	-1.8	0.6	2.58	0.02	2.35	0.02	-10.5	1809	23
DLW1450-08	6.69	0.10	-1.7	0.4	2.90	0.02	2.71	0.02	-9.2	2232	35
DLW1450-09	9.81	0.08	0.6	0.5	2.41	0.02	2.20	0.02	-8.2	1781	31
DLW1450-10	6.53	0.07	-4.9	0.6	2.76	0.02	2.50	0.02	-13.7	1798	29
DLW1450-11	8.04	0.11	-2.2	0.7	2.59	0.03	2.36	0.03	-11.0	1795	31
DLW1450-12	8.72	0.06	-2.7	0.4	2.62	0.02	2.39	0.02	-11.5	1794	26
DLW1450-13	9.94	0.11	-1.1	0.7	2.52	0.03	2.30	0.03	-9.9	1791	39
DLW1450-14	8.22	0.08	1.6	0.9	2.31	0.04	2.11	0.04	-7.4	1725	36
DLW1450-15	7.54	0.08	-4.5	0.7	2.74	0.03	2.48	0.03	-13.2	1800	32
DLW1450-16	8.87	0.14	n.d	n.d	n.d	n.d	n.d	n.d	n.d	1933	32
DLW1450-17	5.60	0.08	-5.3	0.7	2.77	0.03	2.50	0.03	-14.1	1776	35
DLW1450-18	7.75	0.11	-5.3	0.6	2.79	0.02	2.53	0.02	-14.0	1806	31
DLW1450-19	10.0	0.09	-0.3	0.7	2.48	0.03	2.27	0.03	-9.0	1800	33
DLW1450-20	9.20	0.06	-4.9	0.5	2.69	0.02	2.42	0.02	-13.9	1703	39
DLW1450-21	9.11	0.06	-2.2	0.5	2.56	0.02	2.32	0.02	-11.1	1746	31
DLW1450-22	8.54	0.09	-2.1	0.7	2.53	0.03	2.29	0.03	-11.0	1724	31
DLW1450-23	10.34	0.08	n.d	n.d	n.d	n.d	n.d	n.d	n.d	1840	34
DLW1450-24	9.70	0.08	2.5	0.7	2.85	0.03	2.73	0.03	-4.2	1870	35
DLW1450-25	7.50	0.08	n.d	n.d	n.d	n.d	n.d	n.d	n.d	2508	32
DLW1450-26	8.95	0.07	n.d	n.d	n.d	n.d	n.d	n.d	n.d	1761	34
DLW1450-27	9.34	0.09	n.d	n.d	n.d	n.d	n.d	n.d	n.d	1800	35
DLW1450-28	7.89	0.08	-5.7	0.6	2.81	0.02	2.54	0.02	-14.5	1794	31
DLW1450-29	8.30	0.09	-10.6	0.7	3.06	0.03	2.73	0.03	-19.5	1729	31
DLW1450-30	9.04	0.06	-3.1	0.6	2.63	0.03	2.38	0.03	-11.9	1767	33
DLW1450-31	5.56	0.07	2.0	0.7	3.58	0.03	3.51	0.03	-2.2	3400	24
DLW1450-32	8.57	0.08	n.d	n.d	n.d	n.d	n.d	n.d	n.d	1833	79
DLW1450-33	9.05	0.11	-2.1	0.7	2.55	0.03	2.31	0.03	-11.0	1746	39
DLW1450-34	9.92	0.08	3.3	0.5	2.24	0.02	2.06	0.02	-5.5	1776	31
DLW1450-35	9.89	0.08	2.2	0.6	2.26	0.02	2.06	0.02	-6.8	1711	38
DLW1450-36	8.27	0.06	-10.0	0.7	3.05	0.03	2.74	0.03	-18.8	1777	29
DLW1450-37	10.5	0.09	-6.7	0.4	2.88	0.02	2.60	0.02	-15.5	1800	31
DLW1450-38	6.00	0.07	7.3	0.8	2.03	0.03	1.90	0.03	-1.4	1828	28
DLW1450-39	8.89	0.06	-4.7	0.5	2.66	0.02	2.39	0.02	-13.7	1681	39
DLW1450-40	9.18	0.06	-2.0	0.5	2.52	0.02	2.28	0.02	-11.0	1714	34
Sample DLW1412, a sandstone from the Alwar Group, North Delhi Supergroup, N.27°06'04.0" E.76°03'28.5											
DLW1412-01	3.93	0.09	11.0	0.5	1.81	0.02	1.72	0.02	2.4	1844	37
DLW1412-02	8.73	0.09	-5.7	0.5	2.83	0.02	2.57	0.02	-14.4	1828	30
DLW1412-03	7.67	0.07	-3.6	0.6	2.72	0.02	2.48	0.02	-12.2	1850	30
DLW1412-04	8.47	0.10	-8.3	0.5	3.03	0.02	2.74	0.02	-16.8	1876	25
DLW1412-05	6.81	0.07	-5.7	0.6	3.35	0.02	3.14	0.02	-12.4	2506	24
DLW1412-06	7.88	0.08	-6.2	0.6	2.93	0.02	2.67	0.02	-14.7	1909	7
DLW1412-07	9.65	0.08	-6.8	1.1	2.95	0.04	2.68	0.04	-15.2	1896	31
DLW1412-08	5.59	0.08	5.2	0.6	2.27	0.02	2.13	0.02	-3.0	1972	37
DLW1412-09	6.21	0.09	-5.3	0.6	3.47	0.02	3.28	0.02	-11.5	2690	30
DLW1412-10	8.23	0.09	0.1	0.5	2.50	0.02	2.30	0.02	-8.4	1861	32
DLW1412-11	8.25	0.06	-5.2	0.6	2.86	0.02	2.61	0.02	-13.6	1915	28
DLW1412-12	7.84	0.09	-4.4	0.5	2.77	0.02	2.53	0.02	-13.0	1857	27
DLW1412-13	5.07	0.08	10.3	0.7	1.84	0.03	1.74	0.03	1.6	1828	32

TABLE 1

(continued)

Sample No.	$\delta^{18}O$		εHf(t)		$T_{(DM2)}$[a]	±s	$T_{(DM)\ AC}$[b]		$\Delta\varepsilon Hf_{AM}$[c]	U-Pb ages[d]	
	‰	±s		±s	Ga		Ga	±s	ε	Ma	1σ
Sample DLW1412, a sandstone from the Alwar Group, North Delhi Supergroup, N.27°06'04.0" E.76°03'28.5"											
DLW1412-14	8.14	0.08	-0.4	0.7	2.45	0.03	2.23	0.03	-9.2	1754	32
DLW1412-15	10.1	0.10	-5.6	0.5	2.85	0.02	2.59	0.02	-14.2	1854	31
DLW1412-16	9.93	0.07	-1.7	0.8	2.56	0.03	2.33	0.03	-10.5	1789	40
DLW1412-17	7.41	0.07	3.4	0.7	2.26	0.03	2.09	0.03	-5.4	1809	34
DLW1412-18	5.20	0.09	6.2	0.5	2.14	0.02	2.00	0.02	-2.4	1872	35
DLW1412-19	5.53	0.06	-1.9	0.6	3.13	0.02	2.96	0.02	-8.6	2517	30
DLW1412-20	10.1	0.09	-4.4	0.6	2.78	0.02	2.53	0.02	-12.9	1861	27
DLW1412-21	10.3	0.06	-5.3	0.5	2.80	0.02	2.54	0.02	-14.0	1817	28
DLW1412-22	8.71	0.06	n.d	n.d	n.d	n.d	n.d	n.d	n.d	1836	30
DLW1412-23	9.44	0.09	-2.0	0.5	2.53	0.02	2.29	0.02	-10.9	1728	33
DLW1412-24	8.62	0.06	-3.1	0.5	2.69	0.02	2.46	0.02	-11.7	1854	42
DLW1412-25	8.65	0.07	n.d	n.d	n.d	n.d	n.d	n.d	n.d	1894	37
DLW1412-26	8.20	0.06	-2.1	0.4	2.64	0.02	2.42	0.02	-10.7	1865	35
DLW1412-27	5.99	0.10	6.1	0.5	2.73	0.02	2.65	0.02	-0.2	2639	26
DLW1412-28	7.96	0.10	-3.0	0.6	3.39	0.02	3.23	0.02	-9.0	2767	24
DLW1412-29	8.33	0.06	-1.1	0.6	2.54	0.02	2.33	0.02	-9.8	1820	30
DLW1412-30	8.55	0.08	-3.8	0.5	2.75	0.02	2.50	0.02	-12.3	1869	33
DLW1412-31	8.74	0.08	n.d	n.d	n.d	n.d	n.d	n.d	n.d	1928	31
DLW1412-32	8.76	0.08	1.0	0.6	2.49	0.02	2.30	0.02	-7.3	1924	33
DLW1412-33	7.19	0.08	-5.5	0.7	3.01	0.03	2.77	0.03	-13.4	2078	37
DLW1412-34	6.61	0.07	1.4	0.5	2.50	0.02	2.32	0.02	-6.9	1967	29
DLW1412-35	9.78	0.08	-2.0	0.6	2.55	0.02	2.32	0.02	-10.9	1759	33
DLW1412-36	8.11	0.06	5.3	0.8	2.16	0.03	2.00	0.03	-3.4	1828	29
DLW1412-37	5.77	0.13	0.2	0.6	2.49	0.02	2.28	0.02	-8.4	1848	28
DLW1412-38	8.51	0.10	-2.6	0.7	2.65	0.03	2.41	0.03	-11.2	1835	26
DLW1412-39	10.1	0.07	-3.5	0.5	2.62	0.02	2.37	0.02	-12.4	1733	39
DLW1412-40	8.65	0.06	-2.5	0.9	2.61	0.03	2.37	0.03	-11.3	1791	30
Sample DLW1473, a sandstone from the Kumbhalgarh Group, South Delhi Supergroup, N.24°45'09.5" E.73°21'31.9"											
DLW1473-01	6.67	0.08	-9.2	0.4	2.55	0.02	2.19	0.02	-19.7	1172	33
DLW1473-02	7.36	0.07	-1.6	0.5	2.43	0.02	2.19	0.02	-10.8	1628	35
DLW1473-03	2.18	0.12	3.0	0.5	1.76	0.02	1.53	0.02	-7.5	1140	44
DLW1473-04	2.34	0.09	1.9	0.4	1.83	0.02	1.58	0.02	-8.7	1131	43
DLW1473-05	7.04	0.08	n.d	n.d	n.d	n.d	n.d	n.d	n.d	1161	33
DLW1473-06	5.82	0.10	-2.3	0.5	2.04	0.02	1.74	0.02	-13.1	1059	31
DLW1473-07	6.59	0.08	6.7	0.6	1.68	0.03	1.50	0.03	-3.3	1329	34
DLW1473-08	1.52	0.10	5.1	0.7	1.62	0.03	1.41	0.03	-5.6	1120	44
DLW1473-09	2.78	0.10	5.4	0.4	1.69	0.02	1.49	0.02	-4.9	1233	50
DLW1473-10	1.92	0.08	-2.5	0.6	2.16	0.02	1.87	0.02	-12.9	1203	31
DLW1473-11	5.76	0.06	1.9	0.4	1.87	0.02	1.63	0.02	-8.6	1187	43
DLW1473-12	4.58	0.06	-7.1	0.4	2.40	0.02	2.06	0.02	-17.6	1155	37
DLW1473-13	7.61	0.10	11.0	0.5	1.40	0.02	1.26	0.02	0.8	1307	44
DLW1473-14	5.96	0.07	1.2	0.4	1.94	0.02	1.69	0.02	-9.2	1218	42
DLW1473-15	6.43	0.07	11.2	1.4	2.41	0.05	2.38	0.05	4.8	2627	26
DLW1473-16	9.19	0.08	n.d	n.d	n.d	n.d	n.d	n.d	n.d	1648	34
DLW1473-17	6.16	0.09	7.3	0.4	1.78	0.01	1.62	0.01	-2.3	1503	44
DLW1473-18	2.11	0.06	4.9	0.5	1.68	0.02	1.47	0.02	-5.6	1176	36
DLW1473-19	6.31	0.09	4.2	0.4	1.78	0.02	1.57	0.02	-6.1	1257	47
DLW1473-20	5.96	0.06	11.8	0.7	1.25	0.03	1.11	0.03	1.3	1177	30
DLW1473-21	7.11	0.08	-9.8	0.4	2.55	0.02	2.17	0.02	-20.5	1120	44
DLW1473-22	6.53	0.09	4.0	0.5	2.03	0.02	1.85	0.02	-5.4	1567	36
DLW1473-23	7.78	0.10	6.0	0.6	1.89	0.02	1.72	0.02	-3.4	1548	28
DLW1473-24	6.88	0.07	-11.4	0.5	2.69	0.02	2.30	0.02	-21.9	1172	33
DLW1473-25	7.71	0.11	-7.6	0.5	2.87	0.02	2.58	0.02	-16.5	1732	37
DLW1473-26	7.74	0.08	8.1	0.5	1.75	0.02	1.60	0.02	-1.4	1531	37

TABLE 1
(continued)

Sample No.	$\delta^{18}O$		εHf(t)		$T_{(DM2)}$[a]	±s	$T_{(DM)\ AC}$[b]		$\Delta\varepsilon Hf_{AM}$[c]	U-Pb ages[d]	
	‰	±s		±s	Ga		Ga	±s	ε	Ma	1σ
Sample DLW1473, a sandstone from the Kumbhalgarh Group, South Delhi Supergroup, N.24°45'09.5" E.73°21'31.9"											
DLW1473-27	7.10	0.06	5.5	0.5	1.61	0.02	1.40	0.02	-5.1	1131	29
DLW1473-28	6.59	0.09	n.d	n.d	n.d	n.d	n.d	n.d	n.d	1174	43
DLW1473-29	8.11	0.07	-4.1	0.4	2.28	0.02	1.97	0.02	-14.5	1228	30
DLW1473-30	7.83	0.07	6.8	0.7	1.99	0.03	1.84	0.03	-2.2	1731	30
DLW1473-31	5.84	0.06	-0.6	0.4	2.02	0.02	1.75	0.02	-11.1	1181	35
DLW1473-32	7.81	0.07	5.6	0.6	1.95	0.02	1.78	0.02	-3.7	1584	33
DLW1473-33	6.08	0.08	2.5	0.6	1.90	0.02	1.67	0.02	-7.8	1265	44
DLW1473-34	7.18	0.12	1.8	0.7	1.81	0.03	1.56	0.03	-8.9	1106	36
DLW1473-35	6.35	0.09	6.8	0.4	1.91	0.02	1.76	0.02	-2.4	1631	17
DLW1473-36	6.67	0.10	0.1	0.4	2.08	0.02	1.83	0.02	-10.0	1314	48
DLW1473-37	4.55	0.10	-0.6	0.5	2.03	0.02	1.76	0.02	-11.0	1195	31
DLW1473-38	7.62	0.07	9.2	0.5	1.28	0.02	1.11	0.02	-1.7	1018	40
DLW1473-39	6.78	0.07	n.d	n.d	n.d	n.d	n.d	n.d	n.d	1013	41
DLW1473-40	9.63	0.09	2.0	0.5	2.00	0.02	1.77	0.02	-7.9	1359	31
Sample RJW1427, a conglomerate from the Sindreth Group, N.24°50'01.7" E.72°47'16.4"											
RJW1427-01	n.d	n.d	n.d	n.d	2.39	0.02	n.d	n.d	n.d	907	7
RJW1427-02	8.97	0.06	-8.1	0.4	2.24	0.01	1.86	0.01	-19.5	852	8
RJW1427-03	9.87	0.08	1.3	0.5	2.93	0.02	2.80	0.02	-5.4	2515	35
RJW1427-04	5.56	0.07	6.2	0.5	1.81	0.02	1.64	0.02	-3.5	1456	54
RJW1427-05	5.48	0.08	-3.3	0.5	2.61	0.02	2.36	0.02	-12.2	1729	31
RJW1427-06	5.87	0.06	n.d	n.d	n.d	n.d	n.d	n.d	n.d	2454	41
RJW1427-07	6.20	0.10	2.7	0.5	2.84	0.02	2.71	0.02	-4.0	2506	28
RJW1427-08	5.78	0.11	1.0	0.4	2.96	0.01	2.82	0.01	-5.7	2529	31
RJW1427-09	9.36	0.09	-4.8	0.6	2.08	0.02	1.74	0.02	-16.0	914	7
RJW1427-10	8.95	0.06	-7.0	0.6	2.19	0.02	1.82	0.02	-18.4	875	6
RJW1427-11	9.03	0.06	-8.6	0.4	2.28	0.02	1.89	0.02	-19.9	863	6
RJW1427-12	8.94	0.06	-3.3	0.5	1.96	0.02	1.63	0.02	-14.6	874	6
RJW1427-13	8.81	0.09	-5.5	0.6	2.11	0.02	1.76	0.02	-16.8	897	6
RJW1427-14	5.84	0.07	n.d	n.d	n.d	n.d	n.d	n.d	n.d	2020	36
RJW1427-15	9.28	0.08	-27.0	0.4	3.44	0.02	2.84	0.02	-38.3	885	6
RJW1427-16	12.6	0.09	15.7	0.5	1.53	0.02	1.49	0.02	7.1	1857	39
RJW1427-17	6.25	0.08	3.1	0.5	2.85	0.02	2.73	0.02	-3.5	2554	36
RJW1427-18	8.99	0.06	-7.6	0.4	2.24	0.02	1.86	0.02	-18.8	894	6
RJW1427-19	-3.67	0.07	0.0	0.4	3.17	0.01	3.03	0.01	-6.2	2714	29
RJW1427-20	6.90	0.10	-2.6	0.4	2.76	0.02	2.54	0.02	-10.9	1976	28
RJW1427-21	7.47	0.09	3.3	0.6	2.85	0.02	2.74	0.02	-3.3	2566	32
RJW1427-22	7.93	0.09	-3.3	0.4	2.66	0.02	2.41	0.02	-12.1	1791	37
RJW1427-23	9.36	0.06	-6.8	0.3	2.19	0.01	1.83	0.01	-18.0	896	8
RJW1427-24	6.05	0.13	-5.9	0.3	4.33	0.01	3.56	0.01	-53.4	852	7
RJW1427-25	6.07	0.08	3.1	0.4	2.81	0.02	2.69	0.02	-3.6	2502	67
RJW1427-26	6.37	0.11	-3.1	0.4	3.17	0.02	2.99	0.02	-9.9	2480	29
RJW1427-27	6.14	0.08	-2.2	0.6	3.12	0.02	2.95	0.02	-9.0	2484	32
RJW1427-28	9.19	0.08	n.d	n.d	n.d	n.d	n.d	n.d	n.d	807	8
RJW1427-29	5.71	0.09	-5.5	0.4	3.30	0.01	3.09	0.01	-12.3	2455	26
RJW1427-30	5.41	0.08	3.4	0.5	1.83	0.02	1.61	0.02	-6.9	1255	40
RJW1427-31	9.37	0.09	-4.6	0.5	2.06	0.02	1.72	0.02	-15.8	907	6
RJW1427-32	6.04	0.09	-3.5	0.4	3.16	0.02	2.97	0.02	-10.4	2435	36
RJW1427-33	9.02	0.08	n.d	n.d	n.d	n.d	n.d	n.d	n.d	900	6
RJW1427-34	5.51	0.07	6.7	1.0	2.56	0.04	2.47	0.04	-0.2	2457	38
RJW1427-35	3.67	0.07	8.1	0.6	1.61	0.02	1.44	0.02	-1.9	1344	34
RJW1427-36	7.89	0.08	-7.8	0.6	2.26	0.03	1.88	0.03	-19.0	903	5

TABLE 1

(continued)

Sample No.	$\delta^{18}O$		εHf(t)		$T_{(DM2)}$[a]	±s	$T_{(DM)\ AC}$[b]		$\Delta\varepsilon Hf_{AM}$[c]	U-Pb ages[d]	
	‰	±s		±s	Ga		Ga	±s	ε	Ma	1σ
Sample RJW1427, a conglomerate from the Sindreth Group, N.24°50'01.7" E.72°47'16.4"											
RJW1427-37	9.39	0.10	2.3	0.6	2.10	0.02	1.89	0.02	-7.2	1517	30
RJW1427-38	9.10	0.09	n.d	n.d	n.d	n.d	n.d	n.d	n.d	821	7
RJW1427-39	9.23	0.10	n.d	n.d	n.d	n.d	n.d	n.d	n.d	928	6
RJW1427-40	7.57	0.08	-5.4	0.5	3.61	0.02	3.44	0.02	-11.1	2872	15
RJW1427-41	7.04	0.08	-4.3	0.5	2.51	0.02	2.23	0.02	-13.8	1522	20
RJW1427-42	11.1	0.06	-6.2	0.6	2.12	0.03	1.75	0.03	-17.6	843	4
RJW1427-43	6.43	0.10	1.0	0.7	2.92	0.03	2.78	0.03	-5.9	2476	24
RJW1427-44	9.13	0.06	-0.5	0.5	2.41	0.02	2.54	0.02	-14.2	1692	10
RJW1427-45	8.45	0.08	-5.5	0.6	2.81	0.02	2.18	0.02	-9.5	1813	16
RJW1427-46	5.67	0.09	-9.1	0.5	3.53	0.02	3.29	0.02	-16.0	2465	11
RJW1427-47	6.28	0.06	5.2	0.5	2.06	0.02	1.90	0.02	-3.8	1698	22
RJW1427-48	8.88	0.07	-5.9	0.5	2.09	0.02	1.73	0.02	-17.4	832	5
RJW1427-49	7.41	0.06	-0.7	0.6	2.51	0.02	2.30	0.02	-9.4	1810	26
RJW1427-50	10.6	0.10	n.d	n.d	n.d	n.d	n.d	n.d	n.d	612	7
Sample RJW14104 a sandstone from the Nagaur Formation, Marwar Group, N.27°03'54.6" E.73°34'37.4"											
RJW14104-01	6.99	0.07	-8.4	0.4	2.24	0.02	1.84	0.02	-19.9	821	7
RJW14104-02	8.42	0.10	4.0	0.6	1.44	0.02	1.19	0.02	-7.6	795	6
RJW14104-03	7.43	0.08	1.6	0.6	2.87	0.02	2.73	0.02	-5.3	2461	33
RJW14104-04	8.72	0.10	n.d	n.d	n.d	n.d	n.d	n.d	n.d	847	8
RJW14104-05	7.40	0.10	10.9	0.4	1.07	0.02	0.90	0.02	-0.5	873	7
RJW14104-06	6.64	0.09	1.7	0.7	2.86	0.03	2.72	0.03	-5.2	2452	24
RJW14104-07	6.35	0.11	n.d	n.d	n.d	n.d	n.d	n.d	n.d	773	6
RJW14104-08	5.94	0.09	0.3	0.7	2.96	0.03	2.81	0.03	-6.5	2472	29
RJW14104-09	7.01	0.09	-7.2	0.6	2.84	0.02	2.55	0.02	-16.1	1722	39
RJW14104-10	8.53	0.07	1.9	0.6	2.33	0.02	2.14	0.02	-6.9	1783	30
RJW14104-11	7.38	0.07	n.d	n.d	n.d	n.d	n.d	n.d	n.d	683	7
RJW14104-12	7.99	0.07	-5.2	0.6	2.70	0.02	2.43	0.02	-14.2	1694	44
RJW14104-13	7.76	0.08	4.4	0.6	1.41	0.02	1.16	0.02	-7.1	793	6
RJW14104-14	7.32	0.10	n.d	n.d	n.d	n.d	n.d	n.d	n.d	898	2565
RJW14104-15	6.59	0.06	1.8	0.6	1.74	0.02	1.49	0.02	-9.1	1017	31
RJW14104-16	7.04	0.07	4.4	0.5	1.39	0.02	1.14	0.02	-7.2	771	7
RJW14104-17	8.10	0.08	n.d	n.d	n.d	n.d	n.d	n.d	n.d	772	6
RJW14104-18	7.77	0.07	2.7	0.6	2.28	0.02	2.10	0.02	-6.1	1783	46
RJW14104-19	5.37	0.08	-9.5	0.8	3.25	0.03	2.97	0.03	-17.4	2078	29
RJW14104-20	5.73	0.10	2.3	0.6	1.60	0.02	1.33	0.02	-9.0	865	10
RJW14104-21	5.80	0.06	n.d	n.d	n.d	n.d	n.d	n.d	n.d	795	9
RJW14104-22	8.51	0.08	n.d	n.d	n.d	n.d	n.d	n.d	n.d	820	8
RJW14104-23	6.33	0.09	4.8	0.5	1.38	0.02	1.13	0.02	-6.8	777	6
RJW14104-24	7.48	0.07	-5.5	0.9	2.69	0.04	2.42	0.04	-14.6	1666	52
RJW14104-25	7.33	0.08	-12.6	0.7	3.68	0.03	3.40	0.03	-19.6	2394	46
RJW14104-26	7.20	0.07	4.9	0.5	1.38	0.02	1.14	0.02	-6.7	794	6
RJW14104-27	7.75	0.07	-0.7	0.6	1.88	0.02	1.59	0.02	-11.7	990	7
RJW14104-28	8.06	0.07	n.d	n.d	n.d	n.d	n.d	n.d	n.d	813	7
RJW14104-29	7.78	0.06	-4.4	0.9	2.67	0.03	2.41	0.03	-13.4	1721	40
RJW14104-30	7.97	0.10	4.1	0.9	1.43	0.04	1.18	0.04	-7.5	788	16
RJW14104-31	2.71	0.06	n.d	n.d	n.d	n.d	n.d	n.d	n.d	818	7
RJW14104-32	8.97	0.06	-2.6	0.6	2.58	0.02	2.34	0.02	-11.5	1747	40
RJW14104-33	8.05	0.11	4.8	0.6	1.39	0.02	1.14	0.02	-6.8	789	7
RJW14104-34	7.14	0.07	2.8	0.8	2.24	0.03	2.05	0.03	-6.1	1737	37
RJW14104-35	8.21	0.08	4.2	1.6	1.44	0.06	1.19	0.06	-7.4	805	6
RJW14104-36	7.20	0.10	-8.6	0.6	2.38	0.02	2.01	0.02	-19.6	996	8

TABLE 1

(continued)

Sample No.	$\delta^{18}O$		εHf(t)		$T_{(DM2)}$[a]	±s	$T_{(DM)\ AC}$[b]		$\Delta\varepsilon Hf_{AM}$[c]	U-Pb ages[d]	
	‰	±s		±s	Ga		Ga	±s	ε	Ma	1σ
Sample RJW14104 a sandstone from the Nagaur Formation, Marwar Group, N.27°03'54.6" E.73°34'37.4"											
RJW14104-37	8.24	0.10	-0.3	0.6	2.42	0.02	2.20	0.02	-9.2	1725	37
RJW14104-38	8.59	0.06	-0.2	0.6	2.47	0.02	2.25	0.02	-8.9	1792	30
RJW14104-39	6.40	0.06	9.5	1.1	1.08	0.04	0.88	0.04	-2.1	773	7
RJW14104-40	6.28	0.06	n.d	n.d	n.d	n.d	n.d	n.d	n.d	1976	39
RJW14104-41	7.77	0.09	n.d	n.d	n.d	n.d	n.d	n.d	n.d	780	9
RJW14104-42	7.50	0.08	11.4	0.5	2.30	0.02	2.25	0.02	4.7	2494	21
RJW14104-43	7.51	0.08	5.6	0.9	1.46	0.04	1.24	0.04	-5.5	955	35
RJW14104-44	10.4	0.08	4.6	0.6	1.45	0.02	1.21	0.02	-6.7	864	6
RJW14104-45	10.2	0.08	-2.8	0.6	1.99	0.02	1.67	0.02	-13.9	953	7
RJW14104-46	6.47	0.07	14.6	2.2	0.68	0.09	0.54	0.09	2.7	679	5
RJW14104-47	8.38	0.10	-0.3	0.7	2.43	0.03	2.21	0.03	-9.2	1735	30
RJW14104-48	7.23	0.06	5.1	0.6	1.34	0.02	1.10	0.02	-6.5	765	6
RJW14104-49	7.44	0.09	-6.8	0.6	2.80	0.02	2.52	0.02	-15.8	1700	35
RJW14104-50	6.29	0.07	n.d	n.d	n.d	n.d	n.d	n.d	n.d	894	9

[a] Two stage model age in Billion years (Ga) are calculated using the measured $^{176}Lu/^{177}Hf$ of each spot, a value of 0.009 for the bulk Precambrian crust (Vervoort and Jonathan, 1996), and a depleted mantle $^{176}Lu/^{177}Hf$ and $^{176}Hf/^{177}Hf$ of 0.0384 and 0.28325, respectively (see Griffin and others, 2000 for details and references).

[b] $T_{(DM)AC}$ is calculated assuming that new crust was extracted from the arc mantle (Iizuki and others, 2017).

[c] The deviation of εHf(t) between detrital zircons and the arc mantle.

[d] U-Pb ages used for initial Hf calculation refers to $^{207}Pb/^{206}Pb$ age and $^{206}Pb/^{238}U$ ages for zircon older and younger than 1000Ma, respectively.

[e] n.d. means not determined.

zation ages in figure 6. Both Hf isotopic evolution of depleted mantle (DM) (Griffin and others, 2000), new continental crust (Dhuime and others, 2011) and arc mantle are also shown for reference (Iizuka and others, 2013). Only a small fraction of zircon grains (4% of total population) have the Hf isotopic compositions similar to depleted mantle. About 23 percent of zircons plot in the field of arc mantle (fig. 6F). The oldest zircon ($^{207}Pb/^{206}Pb$ age of 3400 ±24 Ma) has $\varepsilon_{Hf(t)}$ value of +2.0, slightly lower than the depleted mantle values but within the range for arc mantle. Zircons within the major age group display variable $\varepsilon_{Hf(t)}$ ranging from sub-chondritic to nearly depleted mantle values (fig. 6F). However, the proportion of mantle-like (related to arc mantle) $\varepsilon_{Hf(t)}$ values vary significantly within each age group. For instance, only 10 percent of zircons in the 1.93 to 1.62 Ga age range have mantle-like Hf isotopic composition as compared to around 30 percent for zircons in both 1.36 to 0.99 Ga and < 0.99 Ga groups. The deviation of $\varepsilon_{Hf(t)}$ among detrital zircon and the arc mantle values can be represented by $\Delta\varepsilon Hf(t)_{AM}$(Iizuka and others, 2013), which is a function of residence time of the reworked continental crust. It is seen that 1.58 to 1.46 Ga and >2.23 Ga zircons have coherent $\Delta\varepsilon Hf(t)_{AM}$,generally less than −15ε (table S4, http://earth.geology.yale.edu/%7eajs/SupplementaryData/2018/Wang). In contrast, other age group zircons define a wider range of $\Delta\varepsilon Hf(t)_{AM}$values that can be as low as −25ε (table S4). Two Neoproterozoic zircon grains from sample RJW1427 have extremely low $\Delta\varepsilon Hf(t)_{AM}$values of −53ε and −38ε, corresponding to Hf model ages of 3.69 Ga and 2.97 Ga, respectively.

O-Isotopic Data

O-isotopic data are summarized in table 1 and illustrated in the zircon crystallization age versus $\delta^{18}O$ diagram (fig. 7). All the analyses have $\delta^{18}O$ values less than 11.1 permil, except for a single grain with 12.6 permil. The Archean and early Paleoproterozoic (>1.9 Ga) zircon grains show relatively restricted range of $\delta^{18}O$

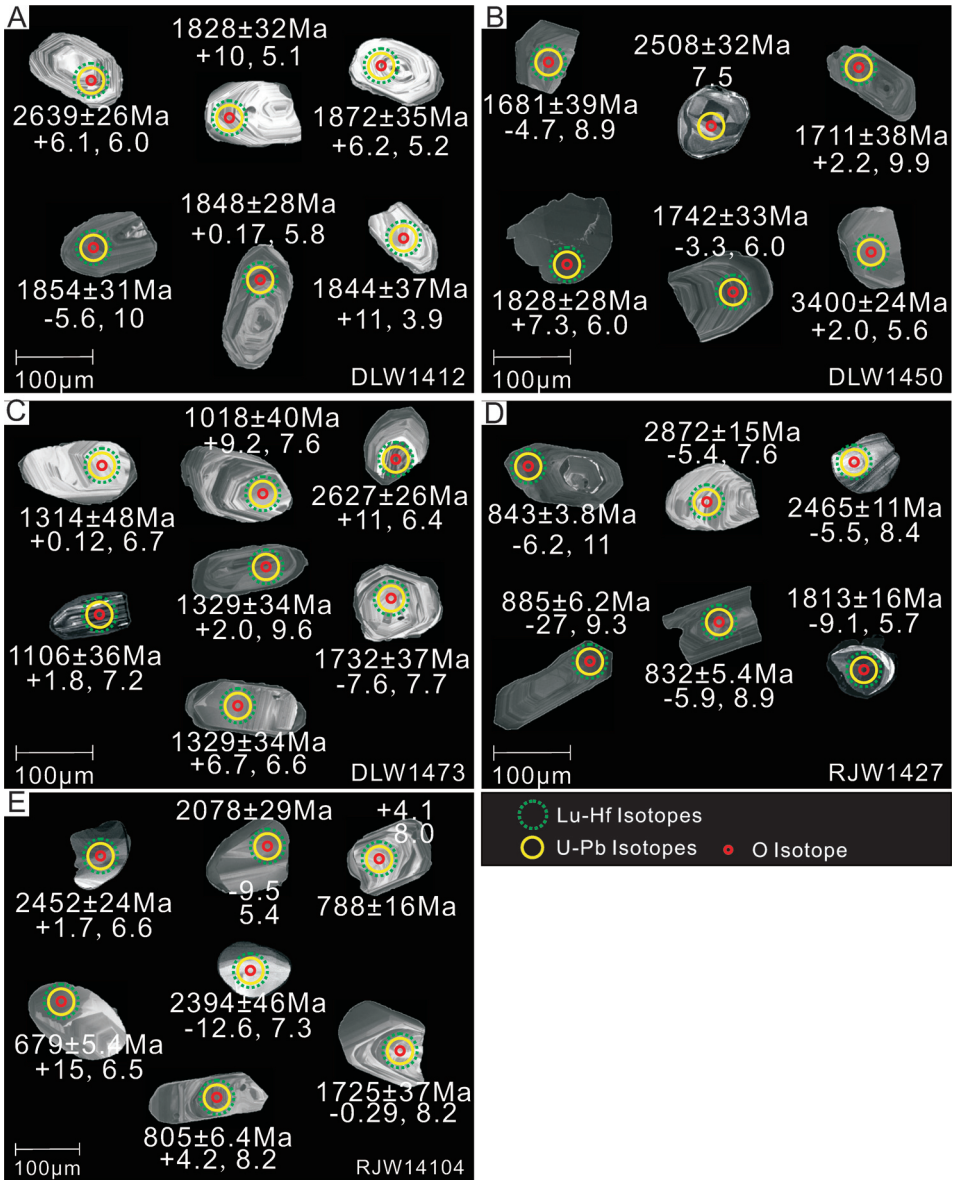

Fig. 3. Representative CL images showing internal structures and external morphology of detrital zircons analyzed in this study. U-Pb ages, $\varepsilon_{Hf(t)}$ and $\delta^{18}O$ values of individual analyzed grain are marked.

values of 8.0 to 5.4 permil, excluding two extreme values of 9.9 permil and −3.7 permil. More variable $\delta^{18}O$ values were observed in zircons younger than 1.9 Ga. Zircon grains from the 1.93 to 1.62 Ga age group have sub-mantle to elevated $\delta^{18}O$ values, with the majority having higher than mantle values. Similar variation is also exhibited by the 0.9 to 0.7 Ga age group with only a few zircon grains displaying mantle-like O-isotopic compositions. A significant decrease in zircon $\delta^{18}O$ values since ~1.6 Ga is observed, however, this trend ceases at ~1.1 Ga. About 25 percent of zircons in this group

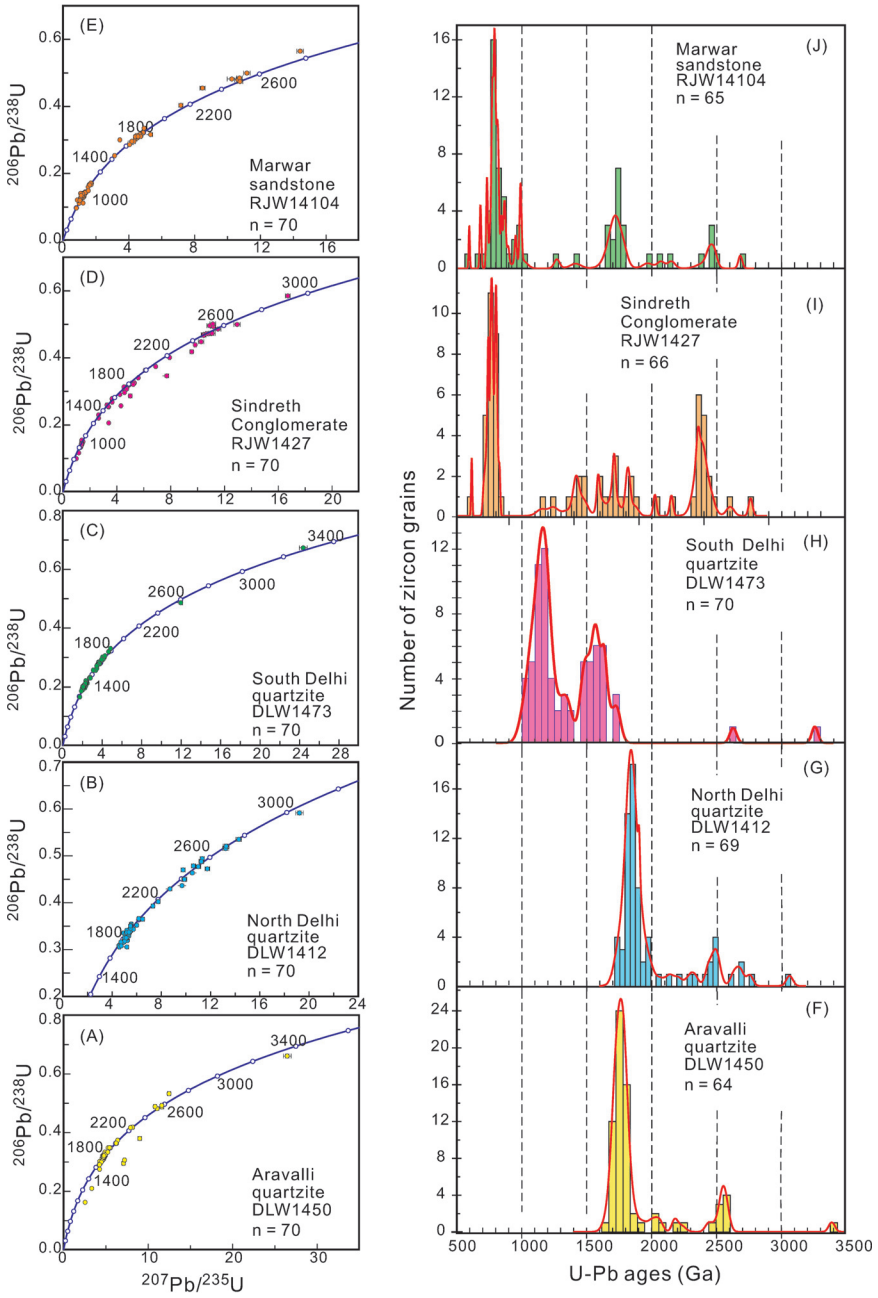

Fig. 4. Concordia plots of U-Pb isotopic compositions (A-E) and U-Pb age histogram (F-J) of detrital zircons from Paleoproterozoic to Early Cambrian sedimentary rocks of NW India. Analyses with concordance between 90% and 110% (table S2, http://earth.geology.yale.edu/%7eajs/SupplementaryData/2018/Wang) have been used in generating the histograms.

have sub-mantle $\delta^{18}O$ values, distinct from the U-Pb and Hf-O data on similar age detrital zircons from other continents (Hawkesworth and Kemp, 2006; Wang and others, 2009; Iizuka and others, 2013).

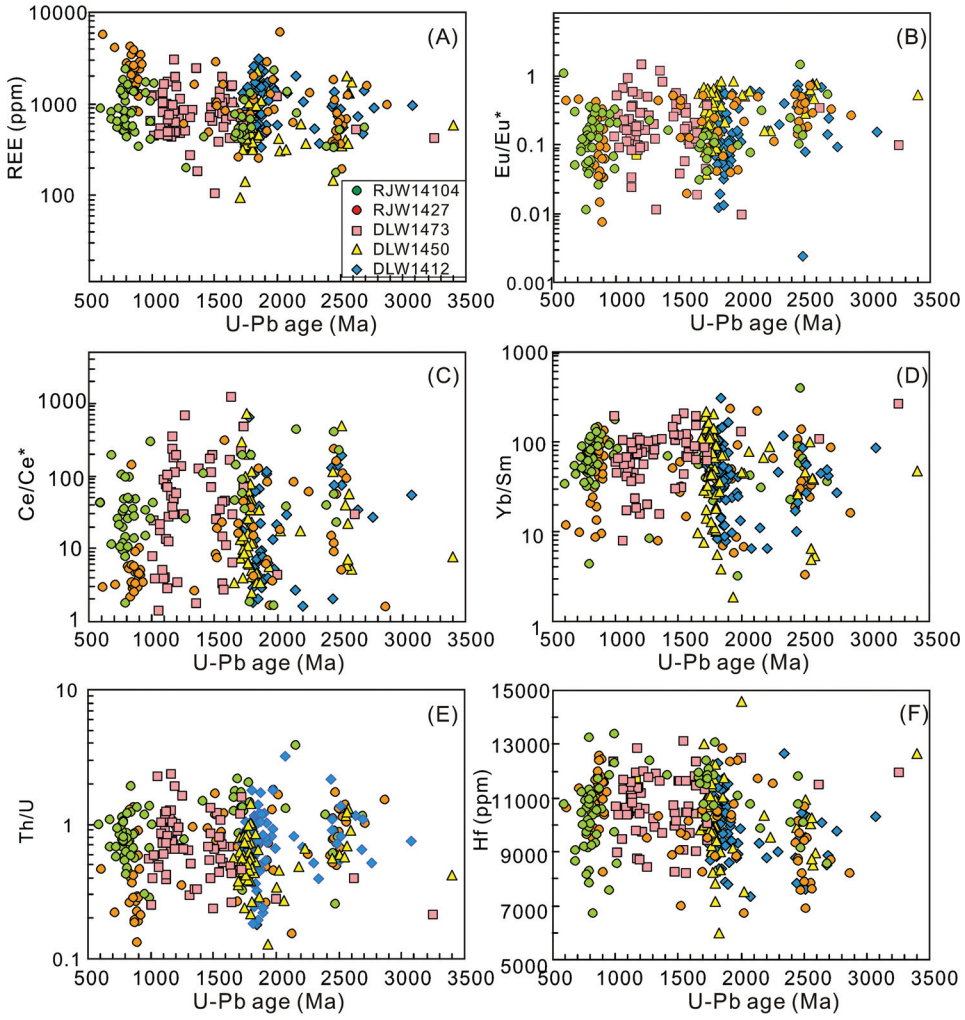

Fig. 5. Diagrams showing trace element compositions of detrital zircon analyzed as a function of their crystallization age.

DISCUSSION

Preservation of Original Isotopic Signatures in Detrital Zircons

Identifying robust and meaningful isotopic data in detrital zircons is important, given the possibility of ancient Pb loss, which would result in $^{207}Pb/^{206}Pb$ ages younger than the true magmatic ages. This would result in disproportionately older Hf model ages and low ε_{Hf} values (Kemp and others, 2009b; Vervoort and Kemp, 2016). All analyzed zircon grains show clear oscillatory zoning and are free from cracks, inclusions and metamict overprint (fig. 3), typical of igneous zircons with no Pb loss. The chondrite normalized patterns for nearly all the zircon grains show rather steep LREE to HREE slopes, positive Ce and negative Eu anomalies that together with their high Th/U ratios, underline igneous origin and rule out any post-crystallization alteration (Hoskin and Schaltegger, 2003; Wu and Zheng, 2004). The younger detrital zircon

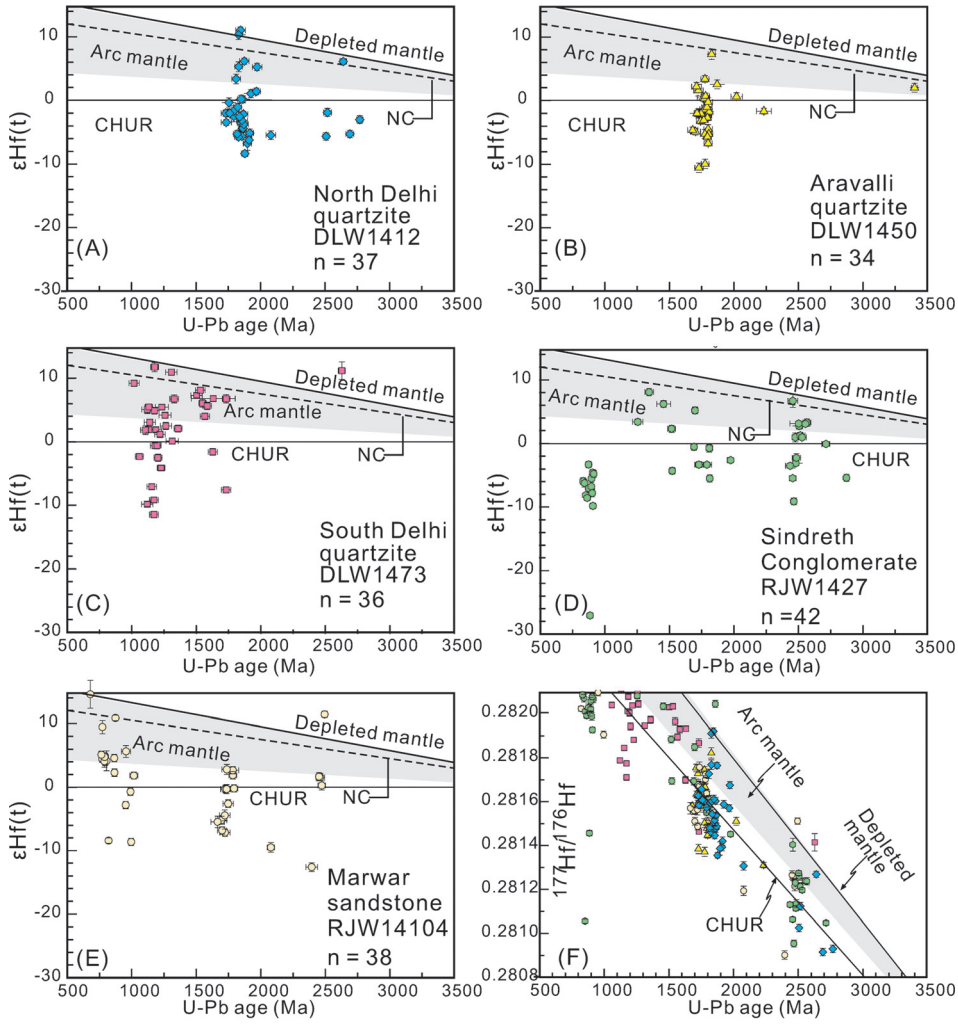

Fig. 6. Plots of $\varepsilon_{Hf(t)}$ versus U-Pb age for detrital zircon from (A) DLW1412, the North Delhi Group, (B) DLW1450, the Aravalli Supergroup, (C) DLW1473, the South Delhi Group, (D) RJW1427, the Sindreth Group, (E) RJW14104, the Marwar Supergroup and (F) initial $^{177}Hf/^{176}Hf$ ratios of all the analyzed samples. One Neoproterozoic zircon ($^{206}Pb/^{238}U$ age = 852 Ma) from sample DLW1427 has extremely low $\varepsilon_{Hf(t)}$ of −42, which is not shown to save space. The Hf isotopic compositions of arc mantle (Iizuka and others, 2013) and new continental curst (NC, Dhuime and others, 2011) are shown for reference.

grains in the present study generally have higher initial $^{177}Hf/^{176}Hf$ ratios, and no clear horizontal trends that could be attributed to ancient Pb loss from a single magmatic zircon component (fig. 6F) (Amelin and others, 2000; Gerdes and Zeh, 2009; Iizuka and others, 2009). Furthermore, the ancient Pb loss has not been recognized in zircons from ~3.3 Ga migmatitic gneiss (BGC) and ~2.6 to 2.4 Ga granitoids in the Aravalli-Delhi Fold Belt as the restricted U-Pb isotopic data underline a single magmatic component (Wiedenbeck and Goswami, 1994; Roy and Kröner, 1996; Wiedenbeck and others, 1996). Therefore, the single growth zone in analyzed zircon domains together with the measured U-Pb ages can be assumed to represent the true crystallization time of zircons, and thus the formation time of the zircon hosting crustal components.

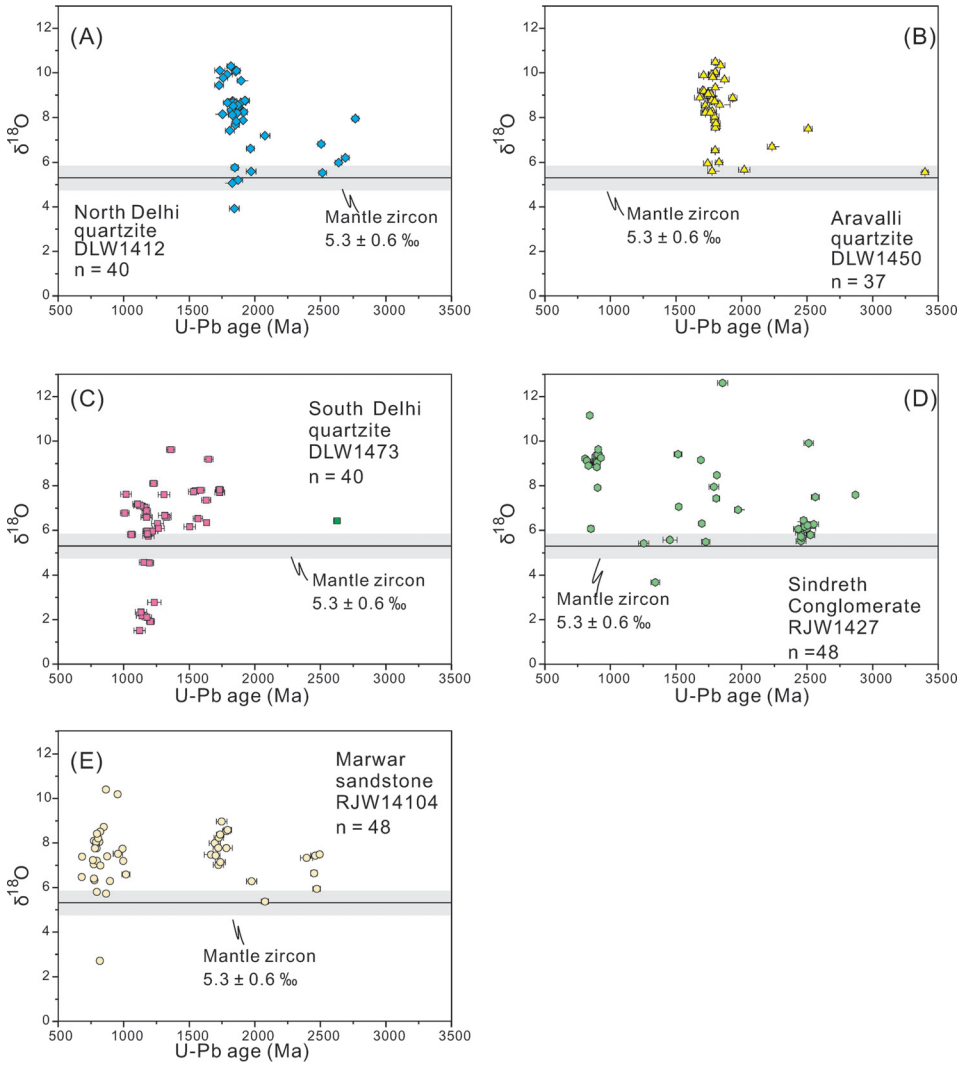

Fig. 7. Plots of $\delta^{18}O$ versus U-Pb age for detrital zircons from (A) DLW1412, the North Delhi Group, (B) DLW1450, the Aravalli Supergroup, (C) DLW1473, the South Delhi Group, (D) RJW1427, the Sindreth Group and (E) RJW14104, the Marwar Supergroup. Gray bands show the $\delta^{18}O$ value of mantle zircon (5.3 ± 0.6‰, Valley and others, 2005). One Neoarchean zircon ($^{207}Pb/^{206}Pb$ age = 2714 Ma) from sample DLW1427 has extremely low-$\delta^{18}O$ of −3.67, which is not shown to save space.

The Timing of Major Continental Generation Episodes

The detrital zircons U-Pb ages exhibit peaks at 2.6 to 2.4, 1.9 to 1.7, 1.2 to 1.0 and 0.9 to 0.7 Ga, which, except for ages between 1.2 Ga and 1.0 Ga (fig. 8A), correlate well with the widely exposed components in NW India (Meert and Pandit, 2015). The 2.6 to 2.4 Ga TTG-like, sanukitoid, and high-K granitoid suites are widely distributed in the southern segment of the Aravalli-Delhi Fold Belt (Wiedenbeck and others, 1996; Rahaman and Mondal, 2015). In contrast, the 1.9 to 1.7 Ga rocks are largely represented by the 1.86 to 1.81 Ga subduction-related and 1.73 to 1.70 Ga extension-related magmatic rocks in the northern segment of the Aravalli-Delhi Fold Belt

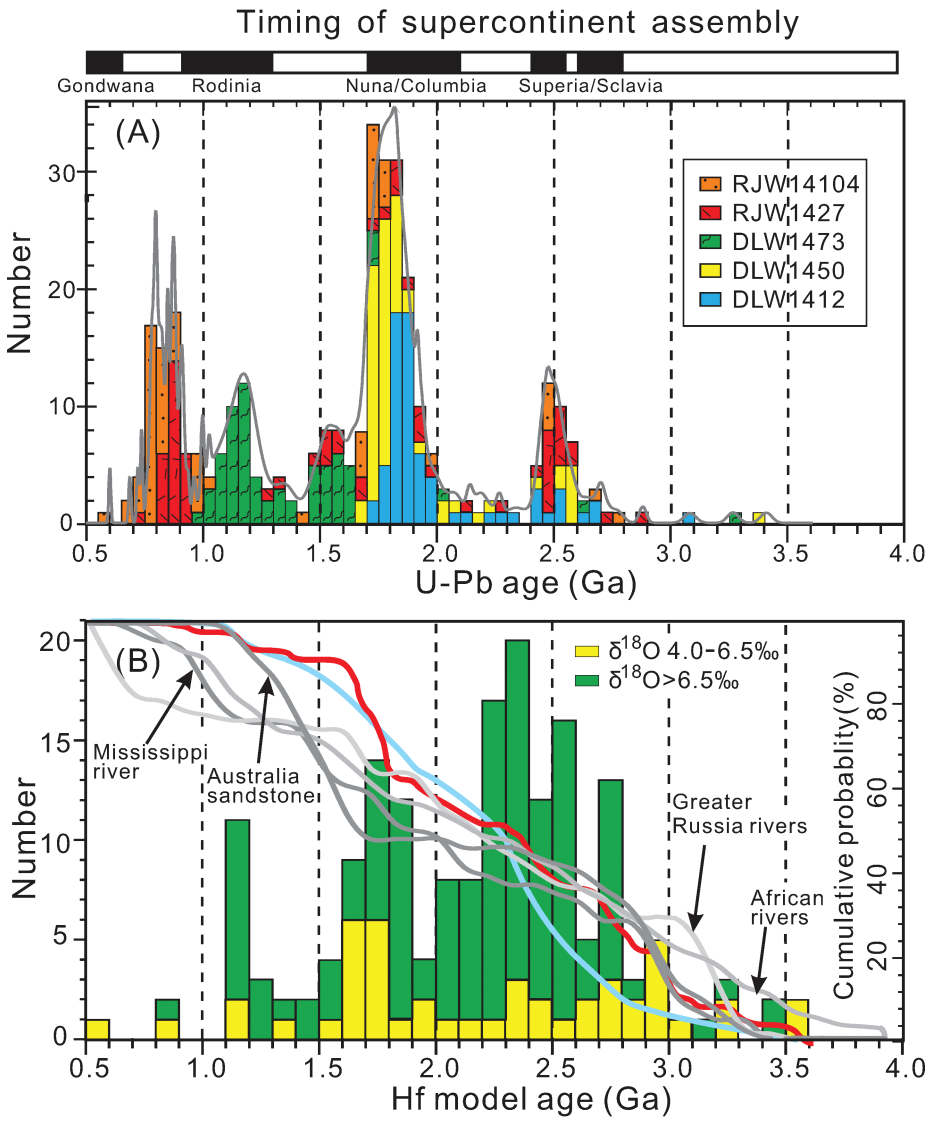

Fig. 8. (A) Combined U-Pb age population of detrital zircon from Paleoproterozoic to Early Cambrian sedimentary rocks. Periods of supercontinent assembly are shown in the top for reference. (B) Hf model ages of zircons with mantle like $\delta^{18}O$ values (yellow bins) represent periods of juvenile continental crust generation and zircons with elevated $\delta^{18}O$ values (green bins) reflect hybrid model ages. Note that the Hf model ages are calculated using Hf isotopic composition of arc mantle (compare, Iizuka and others, 2013). Cumulative probability curves for zircons with $\delta^{18}O$ of 4.0-6.5‰ (red line) and greater than 6.5‰ (blue line)are also shown. Detrital zircon data from Greater Russian rivers (Wang and others, 2011), African rivers (Iizuka and others, 2013), Mississippi River from North America (Wang and others, 2009) and Australia (Kemp and others, 2006) are also shown for comparison.

(Biju-Sekhar and others, 2003; Dharma Rao and others, 2013; Kaur and others, 2011, 2013, 2017a, 2017b), although there is a ~1.90 Ga synkinematicaly emplaced Darwal granite in the south of the belt (Choudhary and others, 1984). The 0.9 to 0.7 Ga rocks are widely distributed along the boundary between the Marwar Block and the Aravalli-Delhi Fold Belt, as represented by the 870 to 800 Ma Erinpura Granite (Deb and

others, 2001; van Lenteand others, 2009; Singh and others, 2010; Pradhan and others, 2010; Just and others, 2011) and the 780 to 750 Ma Malani Igneous Suite (Torsvik and others, 2001b; Gregory and others, 2009; Meert and others, 2013; Wang and others, 2017b, 2019; de Wall and others, 2018). Zircons with 1.2 to 1.0 Ga ages were, most likely, sourced from pre-existing rocks that are no longer preserved/exposed in NW India. The period 1.2 to 1.0 Ga corresponds with collisional assembly of Rodinia supercontinent, with NW India located either along the periphery of, or on a separate plate to, the supercontinent (Torsvik and others, 2001a; Li and others, 2008; Gregory and others, 2009; Cawood and others, 2013b, 2017; Merdith and others, 2017). In addition, detrital zircon grains of this age bracket are mostly euhedral to subhedral (fig. 3C), suggesting a short-distance transport. Hence, it seems unlikely that the 1.2 to 1.0 Ga detritus were sourced from a terrane outboard of NW India during the deposition of the South Delhi Group, and which was subsequently removed.

The prominent U-Pb age peaks indicate either episodic igneous events or selective preservation of magmatic rocks in certain time period(s) (Condie, 1998; Rino and others, 2004; Hawkesworth and others, 2010; Cawood and others, 2013a). Nearly all the analyzed zircon grains have $\varepsilon_{Hf(t)}$ values lower than the depleted mantle at any given time and only 23 percent of the zircons plot within the range for juvenile crust Hf isotopic composition, indicating crystallization of most zircons from recycled crustal magma sources. For the analyzed age groups at >2.23 Ga, 1.93 to 1.62 Ga, 1.58 to 1.46 Ga, 1.36 to 0.99 Ga and < 0.99 Ga (fig. 9A), zircon grains with mantle-like Hf isotopic compositions occupy 25 percent, 10 percent, 70 percent, 29 percent and 30 percent in each group, respectively.

The Hf model ages of low $\delta^{18}O$ (4.0–6.5‰) zircons may indicate periods of juvenile crust generation as igneous source rocks for these zircon grains can be correlated with specific continental crust forming events (Iizuka and others, 2013). Relatively continuous generation of continental crust from 3.3 to 1.3 Ga with two broad peaks at 3.1 to 2.7 Ga and 1.7 to 1.5 Ga can be recognized in the histogram of Hf model ages for zircon with $\delta^{18}O$ of 4.0 to 6.5 permil (fig. 8B). The broad peak at 3.3 to 2.7 Ga is characterized by continuous formation of juvenile continental crust, which was reworked at 2.6 to 2.4 Ga to generate magmas with evolved and heterogonous Hf values but mantle like O-isotopic compositions (fig. 9). This event is likely recorded in the generation of 2.6 to 2.4 Ga TTG-like, sanukitoid, and high-K granitoid suite by remelting of the 3.3 to 2.9 Ga Banded Gneiss Complex rocks in the southern Aravalli-Delhi Fold Belt (Rahaman and Mondal, 2015). In contrast, crustal generation at 1.7 to 1.5 Ga was restricted to a relatively short time and this juvenile continental crust was continuously reworked later to generate magmas with evolved and homogenous Hf- but mantle like O-isotopic signatures (fig. 9). This time interval is believed to manifest the onset of post-collisional extension induced by slab breakoff in the northern Aravalli-Delhi Fold Belt (Biju-Sekharand others, 2003; Kaur and others, 2011, 2017a), corresponding to the rapid continental crustal generation in a retreating orogenic belt (Kemp and others, 2009a; Collins and others, 2011). These two age peaks are comparable with juvenile detrital zircons from Eastern Australia and North America (Kemp and others, 2009a; Wang and others, 2009; Glen and others, 2011) (fig. 8B), underlining major episodes of juvenile crustal addition.

Zircon grains with $\delta^{18}O$>6.5 permil have Hf model ages that significantly differ from the above age groups (fig. 9). These represent mixtures of materials that separated from the depleted mantle during earlier events. The 1.9 to 1.7 Ga magmatic episodes do not involve generation of new continental crust because these crystallization ages are not consistent with the Hf crust formation ages (fig. 8B). The 1.9 to 1.7 Ga zircon grains are inferred to contain significant contributions from sediments and their Hf model ages may reflect mixing rather than specific continental crust forming

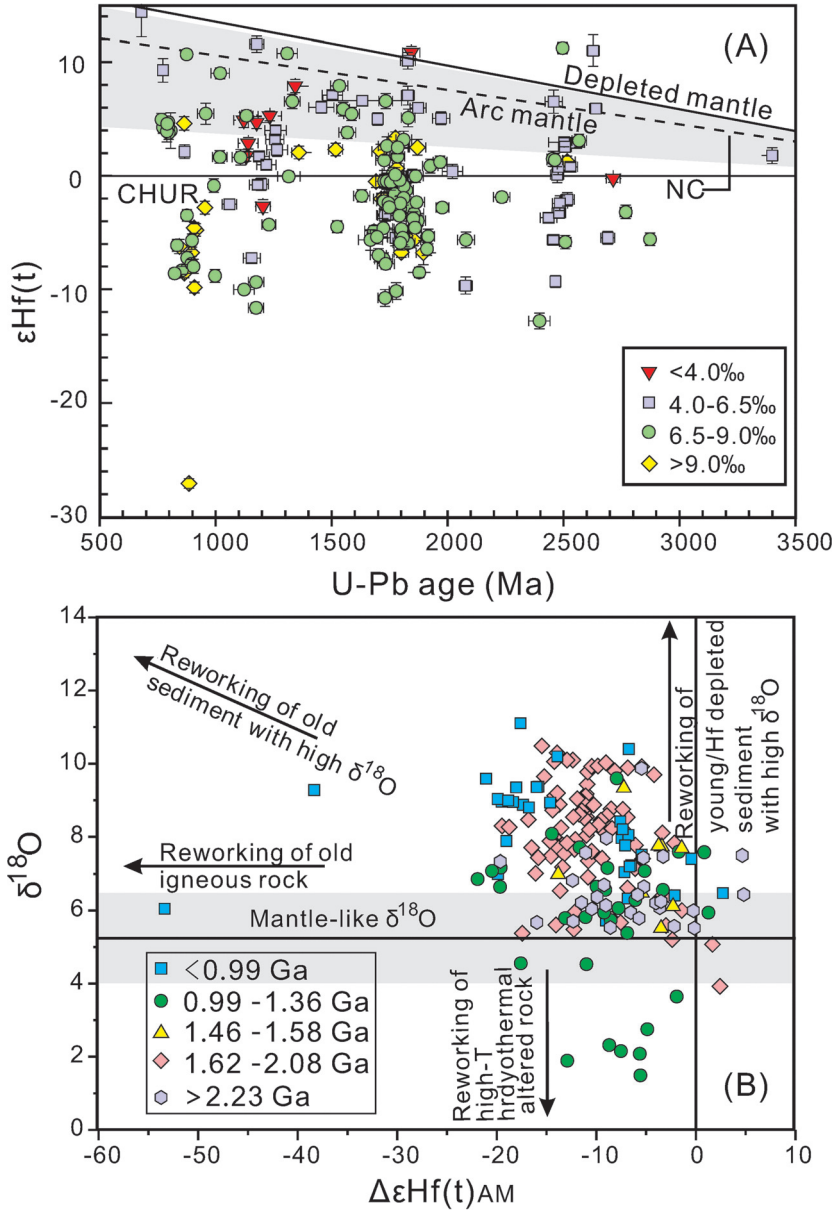

Fig. 9. Systematic U-Pb, Lu-Hf and O isotope data for detrital zircon from all the studied samples; (A) plots of $\varepsilon_{Hf(t)}$ versus U-Pb age, contoured for $\delta^{18}O$; (B) contour plot of crystallization age as a function of $\delta^{18}O$ and $\Delta\varepsilon_{Hf(t)AM}$, the deviation of $\varepsilon_{Hf(t)}$ between detrital zircon and the arc mantle (compare Iizuka and others, 2013). The Hf isotopic compositions of arc mantle (Iizuka and others, 2013) and new continental curst (NC, Dhuime and others, 2011) are shown for reference.

events. Similar events are recognized for 1.2 to 1.0 and 0.9 to 0.7 Ga zircons, which indicate that magmatism during these periods was dominated either by reworking of igneous rocks with mantle like $\delta^{18}O$ values or of sediments having elevated $\delta^{18}O$ values (fig. 9). These peaks register magmatic episodes related to crustal reworking or

stabilization, rather than spikes in the rate of new continental crust generation. Although many late Mesoproterozoic orogenic terranes related to Rodinia assembly are thought to represent juvenile crustal additions (Stein and Hofmann, 1994; Condie, 1998), the present study demonstrates that remelting of older and supracrustal rocks was regionally significant during this period, as has also been suggested for rocks of this age in North America and southeast Australia (Valley and others, 2005; Kemp and others, 2006).

Implications on Crustal Evolution and Supercontinent Cycle

A close correspondence between episodic zircon age peaks and the timing of supercontinent assembly has been recognized in detrital zircon populations from different regions of the world (Condie, 1998; Rino and others, 2004; Campbell and Allen, 2008; O'Reilly and others, 2008; Hawkesworth and others, 2010; Iizuka and others, 2010; Cawood and Hawkesworth, 2015). The punctuated age distribution, observed in this study, clearly underline correlation with the supercontinent cycles (fig. 8A). The 1.9 to 1.7 Ga, 1.6 to 1.5 Ga and 1.3 to 1.0 age groups are consistent with the assembly of Nuna and Rodinia supercontinents, respectively, whereas the peak at 0.9 to 0.7 Ga is consistent with the timing of fragmentation of Rodinia, although the magmatic record of fragmentation is less likely to be preserved than that during supercontinental assembly (Hawkesworth and others, 2010; Cawood and others, 2013a). The 2.6 to 2.4 Ga magmatic record corresponds with the ~2.5 Ga Sclavia/Arctica supercontinent/supercraton that includes Laurentia's Slave Craton and other cratons that drifted from it (Bleeker, 2003; Rogers and Santosh, 2003). The role of India in Sclavia is unclear. Pehrsson and others (2013) have tentatively considered peninsular India as part of 'Rae family' that collided together at 2.55 to 2.45 Ga to form the Nunavutia supercraton. However, NW India lacks 2.7 to 2.6 Ga juvenile continental crust formation and the subsequent 2.45 to 2.20 Ga Arrowsmith event that are common in Rae family cratons (Pehrsson and others, 2013). Moreover, most zircon grains older than 2.23 Ga display mantle-like to slightly elevated $\delta^{18}O$ values (8.0–5.4‰) and $\Delta\varepsilon Hf(t)_{AM}$ as low as −20ε (fig. 10B), indicating that magmatism prior to 2.23 Ga was dominated by reworking of igneous rocks with evolved radiogenic isotopic compositions over reworking of mature sedimentary rocks.

The Nuna supercontinent.— Record of Nuna assembly in NW India is well preserved in the dominantly 1.9 to 1.7 Ga age detrital zircons, most of which show variably sub-mantle $\varepsilon_{Hf(t)}$ and evolved ^{18}O signatures ($\delta^{18}O>7.5‰$), reflecting remelting of dominant mature sedimentary rocks over the generation of juvenile igneous rocks (Belousova and others, 2010; Condie and others, 2011; Voice and others, 2011; Roberts, 2012). A distinct detrital age peak of 1.85 Ga and variable, but largely subchrondritic $\varepsilon_{Hf(t)}$ values also suggest significant reworking of ancient continental crust at that time (Kaur and others, 2013). Moreover, successive sedimentation, metamorphism and subduction-related magmatic activities at ~1.86 to 1.81 Ga along the entire northern Indian margin indicate a convergent margin setting in association with the assembly of the Nuna supercontinent (Kaur and others, 2013, 2017b; Wang and others, 2019). Subsequent, less voluminous but more juvenile, magmas since ~1.7 Ga likely reveal the early separation of NW India from the supercontinent, because supercontinental fragmentation is accompanied by crust generation with low preservation potential (Hawkesworth and others, 2010; Roberts, 2012; Cawood and others, 2013a). This interpretation is also supported by the presence of abundant 1.73 to 1.70 Ga, A-type granitic rocks in the northern Aravalli-Delhi Fold Belt, which manifests lithospheric extension in a post-collisional setting triggered by slab break-up in response to the breakup phase of the Nuna supercontinent (Biju-Sekharand others, 2003; Kaur and others, 2011, 2017a). It seems that voluminous continental crust was generated during the 1.58 to 1.46 Ga period in northwestern India, as suggested by

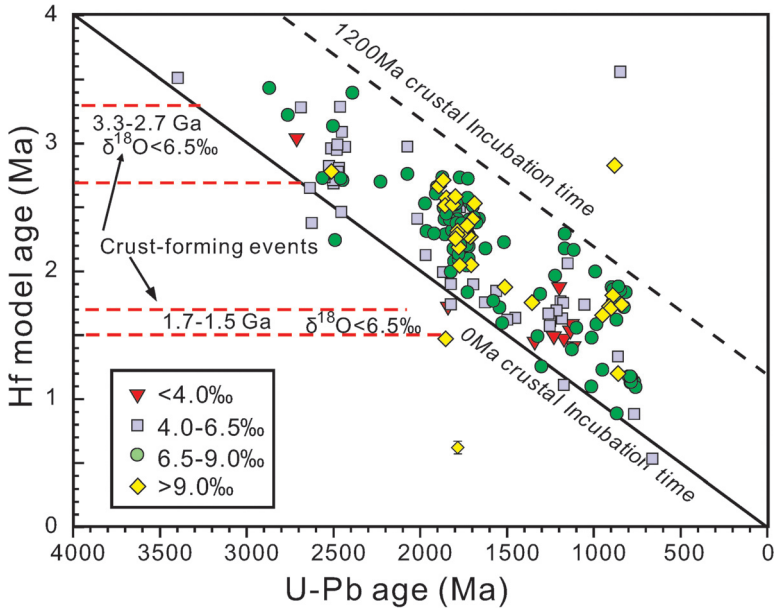

Fig. 10. Hf model ages (T_{DMAC} in table S2, (http://earth.geology.yale.edu/%7eajs/SupplementaryData/2018/Wang) plotted against the U-Pb crystallization ages of zircon, contoured for $\delta^{18}O$. The dashed horizontal red line represents specific periods of crust formation and the diagonal black line indicates 1:1 correspondence between zircon U-Pb crystallization age and the Hf mode ages that is '0 Ma crustal incubation time'.

mantle-like $\varepsilon_{Hf(t)}$ values of zircons. The majority of zircon grains (75%) in this age group also have elevated $\delta^{18}O$ (>6.5‰) value, indicating significant contribution of high $\delta^{18}O$ rocks; either young sediments with mantle-like $\varepsilon_{Hf(t)}$ or carbonate and chert with low Hf contents (compare, Iizuka and others, 2013). The 1.58 to 1.46 Ga detrital zircon grains, however, show trace element characteristics similar to other zircons, such as variable Hf and REE contents, Th/U and Yb/Sm ratios and Ce and Eu anomalies, hinting at insignificant carbonate material in the magma source. Therefore, the mantle-like $\varepsilon_{Hf(t)}$ but elevated $\delta^{18}O$ signatures of 1.58 to 1.46 Ga zircon are likely inherited from young igneous rocks, eroded during rapid uplift of mountain ranges and deposition in basins during continent-continent collision associated with the Nuna assembly at ~2.1 to 1.7 Ga.

The Rodinia supercontinent.—Dominance of 0.9 to 0.7 Ga age group over 1.3 to 1.0 Ga group is the most striking feature of the age distribution patterns in the analyzed samples. This feature observed from northwestern India is in contradiction to the global age compilations that show prominent late Mesoproterozoic (1.3–1.0 Ga) records related to Rodinia assembly and subordinate 0.9 to 0.7 Ga ages related to Rodinia breakup (Campbell and Allen, 2008; Condie and others, 2011; Voice and others, 2011). Moreover, the 0.9 to 0.7 Ga zircon grains show juvenile signatures closely comparable with 1.3 to 1.0 Ga zircons (figs. 9 and 10). These discrepancies underline that peninsular India (assuming that it was unified by 1.0 Ga; Bhowmik and others, 2012) was not located in a position to be actively involved in Rodinia assembly but was more actively involved in Rodinia breakup. —Zircon grains with $\delta^{18}O$ <5.3 permil, in this study, are largely restricted to 1.34 to 1.12 Ga age group (table S4 (http://earth.geology.yale.edu/%7eajs/SupplementaryData/2018/Wang), fig. 11), corresponding to a compressive tectonic regime during the collision between Marwar Block and

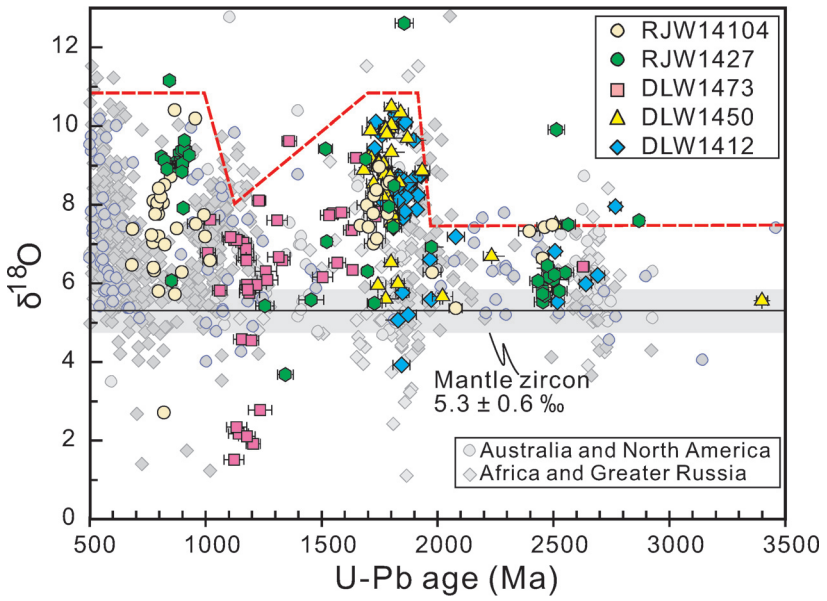

Fig. 11. Plots of $\delta^{18}O$ versus U-Pb age for detrital zircons from Paleoproterozoic to Early Cambrian sedimentary rocks in NW India. Evolution trends of zircon $\delta^{18}O$ versus with time defined by previous studies are also shown for comparison. Detrital zircon data from Greater Russian rivers (Wang and others, 2011), African rivers (Iizuka and others, 2013), Mississippi River from North America (Wang and others, 2009) and Australia (Kemp and others, 2006) are also shown for comparison.

Aravalli - Delhi -BGC terrane, highlighted by the ~1.0 to 0.9 Ga metamorphism, magmatism and tectonism in the Aravalli-Delhi Fold Belt (Pandit and others, 2003; Buick and others, 2006, 2010; Bhowmik and others, 2010; Dharma Rao and others, 2013; Kaur and others, 2016; Ozha and others, 2016). One possible interpretation is that these end Mesoproterozoic low-$\delta^{18}O$ but mantle-like $\varepsilon Hf(t)$ zircons record localized extensional conditions within an overall convergent tectonic setting. Addition of new continental crust is characteristic of an external (accretionary) orogenic system, in contrast to an internal/collision orogen (Collins and others, 2011). Extensional, back-arc rifting episodes in an accretionary orogenic system (Kemp and others, 2009a) would also facilitate water-rock interaction under high temperature. This interpretation on the detrital zircon isotopic signatures provides tacit support to the previous considerations that peninsular India laid either along western periphery of Rodinia or off the supercontinent (Torsvik and others, 2001a; Gregory and others, 2009; Cawood and others, 2013b, 2017; Merdith and others, 2017).

CONCLUSIONS

Generation of continental crust continuously from 3.3 to 1.3 Ga with two broad peaks at 3.3 to 2.7 Ga and 1.7 to 1.5 Ga constrained by Hf model ages of zircon with mantle like $\delta^{18}O$ values is recognized in this study for the NW Indian block. These two peaks represent an Indian example of the global juvenile crustal addition events also recorded in eastern Australia and North America. Prominent U-Pb detrital zircon age peaks in NW India at 1.9 to 1.7 Ga, 1.6 to 1.5 Ga, 1.2 to 1.0 Ga and 0.9 to 0.7 Ga, coincide with the assembly and breakup of Proterozoic supercontinents, Nuna/Columbia and Rodinia. The major magmatic episodes at 1.9 to 1.7 and 1.2 to 1.0 Ga represent significant contributions from sediments rather than juvenile materials,

consistent with major crustal remelting during supercontinent assembly. However, the 0.9 to 0.7 Ga peak, corresponding with fragmentation of Rodinia, documents a magmatic episode of crustal reworking that is in contrast to the generally considered juvenile crustal addition in extensional setting associated with supercontinent breakup. In addition, continental crust generation also occurred during the assembly of Nuna and Rodinia, recorded in the progressive ^{18}O depletion from supra-mantle to mantle values in the 1.7 to 1.5 Ga and 1.34 to 1.12 Ga zircon grains with low $\delta^{18}O$ but high $\varepsilon_{Hf(t)}$ values. This characteristic pattern of crustal evolution differs from the generally accepted global balance between reworking and addition of continental crust, coupled with supercontinent assembly and breakup, and may reflect distinct geodynamic setting and paleoposition for the NW Indian block in the Precambrian supercontinents.

ACKNOWLEDGMENTS

This study was supported by the National Natural Science Foundation of China (NSFC 41572170), "Thousand Youth Talents Plan" grant to Wei Wang, Guangzhou municipal government (201607020029) and MOST Special Fund from the SKLGPMR (MSFGPMR 01-1) and Fundamental Research Funds (CUGCJ1709), China University of Geosciences (Wuhan). WW thanks the Australian Endeavour Research Fellowship 6272_2018 to support his visit to Monash University. Peter A. Cawood acknowledges support from the Australian Research Council grant FL160100168. We would like to thank Zhaochu Hu for (MC)-LA-ICPMS analyses. Terry-Wei and Vivek Kumar Meena are thanked for their generous help during field work. We thank Kent Condie, an anonymous reviewer and the Associate Editor for useful comments and editorial handling that have helped in improving the manuscript.

REFERENCES

Amelin, Y., Lee, D. C., and Halliday, A. N., 2000, Early-middle Archaean crustal evolution deduced from Lu-Hf and U-Pb isotopic studies of single zircon grains: Geochimica et Cosmochimica Acta, v. 64, n. 24, p. 4205–4225, https://doi.org/10.1016/S0016-7037(00)00493-2

Andersen, T., 2002, Correction of common lead in U–Pb analyses that do not report ^{204}Pb: Chemical Geology, v. 192, n. 1–2, p. 59–79, https://doi.org/10.1016/S0009-2541(02)00195-X

Ashwal, L. D., Solanki, A. M., Pandit, M. K., Corfu, F., Hendriks, B. W. H., Burke, K., and Torsvik, T. H., 2013, Geochronology and geochemistry of Neoproterozoic Mt. Abu granitoids, NW India: Regional correlation and implications for Rodinia paleogeography: Precambrian Research, v. 236, p. 265–281, https://doi.org/10.1016/j.precamres.2013.07.018

Belousova, E. A., Kostitsyn, Y. A., Griffin, W. L., Begg, G. C., O'Reilly, S. Y., and Pearson, N. J., 2010, The growth of the continental crust: Constraints from zircon Hf-isotope data: Lithos, v. 119, n. 3–4, p. 457–466, https://doi.org/10.1016/j.lithos.2010.07.024

Bhowmik, S. K., Bernhardt, H.-J., and Dasgupta, S., 2010, Grenvillian age high-pressure upper amphibolite-granulite metamorphism in the Aravalli-Delhi Mobile Belt, Northwestern India: New evidence from monazite chemical age and its implication: Precambrian Research, v. 178, n. 1–4, p. 168–184, https://doi.org/10.1016/j.precamres.2010.02.015

Bhowmik, S. K., Wilde, S. A., Bhandari, A., Pal, T., and Pant, N. C., 2012, Growth of the Greater Indian Landmass and its assembly in Rodinia: Geochronological evidence from the Central Indian Tectonic Zone: Gondwana Research, v. 22, n. 1, p. 54–72, https://doi.org/10.1016/j.gr.2011.09.008

Biju-Sekhar, S., Yokoyama, K., Pandit, M. K., Okudaira, T., Yoshida, M., and Santosh, M., 2003, Late Paleoproterozoic magmatism in Delhi Fold Belt, NW India and its implication: Evidence from EPMA chemical ages of zircons: Journal of Asian Earth Sciences, v. 22, n. 2, p. 189–207, https://doi.org/10.1016/S1367-9120(02)00188-8

Bleeker, W., 2003, The late Archean record: A puzzle in *ca.* 35 pieces: Lithos, v. 71, n. 24, p. 99–134, https://doi.org/10.1016/j.lithos.2003.07.003

Blichert-Toft, J., Chauvel, C., and Albarède, F., 1997, Separation of Hf and Lu for high-precision isotope analysis of rock samples by magnetic sector-multiple collector ICP-MS: Contributions to Mineralogy and Petrology, v. 127, n. 3, p. 248–260, https://doi.org/10.1007/s004100050278

Buick, I. S., Allen, C., Pandit, M., Rubatto, D., and Hermann, J., 2006, The Proterozoic magmatic and metamorphic history of the Banded Gneiss Complex, central Rajasthan, India: LA-ICP-MS U–Pb zircon constraints: Precambrian Research, v. 151, n. 1–2, p. 119–142, https://doi.org/10.1016/j.precamres.2006.08.006

Buick, I. S., Clark, C., Rubatto, D., Hermann, J., Pandit, M., and Hand, M., 2010, Constraints on the Proterozoic evolution of the Aravalli–Delhi Orogenic belt (NW India) from monazite geochronology

and mineral trace element geochemistry: Lithos, v. 120, n. 3–4, p. 511–528, https://doi.org/10.1016/j.lithos.2010.09.011
Campbell, I. H., and Allen, C. M., 2008, Formation of supercontinents linked to increases in atmospheric oxygen: Nature Geoscience, v. 1, p. 554–558, https://doi.org/10.1038/ngeo259
Cawood, P. A., and Hawkesworth, C. J., 2015, Temporal relations between mineral deposits and global tectonic cycles: implications for prospectivity, *in* Jenkin, G. R. T., Lusty, P. A. J., McDonald, I., Smith, M. P., Boyce, A. J., and Wilkinson, J. J., editors, Ore Deposits in an Evolving Earth: Geological Society, London, Special Publications, v. 393, p. 9–21, https://doi.org/10.1144/SP393.1
Cawood, P. A., Hawkesworth, C., and Dhuime, B., 2013a, The continental record and the generation of continental crust: Geological Society of America Bulletin, v. 125, n. 12, p. 14–32, https://doi.org/10.1130/B30722.1
Cawood, P. A., Wang, Y. J., Xu, Y. J., and Zhao, G. C., 2013b, Locating South China in Rodinia and Gondwana: A fragment of greater India lithosphere?: Geology, v. 41, n. 8, p. 903–906, https://doi.org/10.1130/G34395.1
Cawood, P. A., Zhao, G. C., Yao, J. L., Wang, W., Xu, Y. J., and Wang, Y. J., 2017, Reconstructing South China in Phanerozoic and Precambrian supercontinents: Earth Science Reviews, https://doi.org/10.1016/j.earscirev.2017.06.001
Choudhary, A. K., Gopalan, K., and Sastry, C. A., 1984, Present status of the geochronology of the Precambrian rocks of Rajasthan: Tectonophysics, v. 105, n. 1–4, p. 131–140, https://doi.org/10.1016/0040-1951(84)90199-9
Collins, W. J., Belousova, E. A., Kemp, A. I. S., and Murphy, J. B., 2011, Two contrasting Phanerozoic orogenic systems revealed by hafnium isotope data: Nature Geoscience, v. 4, p. 333–337, https://doi.org/10.1038/ngeo1127
Condie, K. C., 1998, Episodic continental growth and supercontinents: A mantle avalanche connection?: Earth and Planetary Science Letters, v. 163, n. 1–4, . 97–108, https://doi.org/10.1016/S0012-821X(98)00178-2
Condie, K. C., Beyer, E., Belousova, E., Griffin, W. L., and O'Reilly, S. Y., 2005, U–Pb isotopic ages and Hf isotopic composition of single zircons: The search for juvenile Precambrian continental crust: Precambrian Research, v. 139, n. 1–2, p. 42–100, https://doi.org/10.1016/j.precamres.2005.04.006
Condie, K. C., Bickford, M. E., Aster, R. C., Belousova, E., and Scholl, D. W., 2011, Episodic zircon ages, Hf isotopic composition, and the preservation rate of continental crust: Geological Society of America Bulletin, v. 123, n. 5–6, p. 951–957, https://doi.org/10.1130/B30344.1
de Wall, H., Pandit, M. K., Dotzler, R., and Just, J., 2012, Cryogenian transpression and granite intrusion along the western margin of Rodinia (Mt. Abu region): Magnetic fabric and geochemical inferences on Neoproterozoic geodynamics of the NW Indian block: Tectonophysics, v. 554–557, p. 143–158, https://doi.org/10.1016/j.tecto.2012.05.022
de Wall, H., Pandit, M. K., Donhauser, I., Schöbel, S., Wang, W., and Sharma, K. K., 2018, Evolution and tectonic setting of the Malani - Nagarparkar Igneous Suite: A Neoproterozoic Silicic-dominated Large Igneous Province in NW India-SE Pakistan: Journal of Asian Earth Sciences, v. 160, p. 136–158, https://doi.org/10.1016/j.jseaes.2018.04.016
Deb, M., Thorpe, R. I., Krstic, D., Corfu, F., and Davis, D. W., 2001, Zircon U-Pb and galena Pb isotope evidence for an approximate 1.0 Ga terrane constituting the western margin of the Aravalli-Delhi orogenic belt, northwestern India: Precambrian Research, v. 108, n. 3–4, p. 195–213, https://doi.org/10.1016/S0301-9268(01)00134-6
Deb, M., Thorpe, R., and Krstic, D., 2002, Hindoli Group of Rocks in the Eastern Fringe of the Aravalli-Delhi Orogenic Belt-Archean Secondary Greenstone Belt or Proterozoic Supracrus tals?: Gondwana Research, v. 5, n. 4, p. 879–883, https://doi.org/10.1016/S1342-937X(05)70922-9
Dharma Rao, C. V., Santosh, M., and Kim, S. W., 2012, Cryogenian volcanic arc in the NW Indian Shield: Zircon SHRIMP U–Pb geochronology of felsic tuffs and implications for Gondwana assembly: Gondwana Research, v. 22, n. 1, p. 36–53, https://doi.org/10.1016/j.gr.2011.10.014
Dharma Rao, C. V., Santosh, M., Kim, S. W., and Li, S., 2013, Arc magmatism in the Delhi Fold Belt: SHRIMP U–Pb zircon ages of granitoids and implications for Neoproterozoic convergent margin tectonics in NW India: Journal of Asian Earth Sciences, v. 78, p. 83–99, https://doi.org/10.1016/j.jseaes.2012.09.007
Dhuime, B., Hawkesworth, C., and Cawood, P., 2011, When Continents Formed: Science, v. 331, n. 6014, p. 154–155, https://doi.org/10.1126/science.1201245
Gerdes, A., and Zeh, A., 2009, Zircon formation versus zircon alteration—New insights from combined U–Pb and Lu–Hf *in-situ* LA-ICP-MS analyses, and consequences for the interpretation of Archean zircon from the Central Zone of the Limpopo Belt: Chemical Geology, v. 261, n. 3–4, p. 230–243, https://doi.org/10.1016/j.chemgeo.2008.03.005
Glen, R. A., Saeed, A., Quinn, C. D., and Griffin, W. L., 2011, U–Pb and Hf isotope data from zircons in the Macquarie Arc, Lachlan Orogen: Implications for arc evolution and Ordovician palaeogeography along part of the east Gondwana margin: Gondwana Research, v. 19, n. 3, p. 670–685, https://doi.org/10.1016/j.gr.2010.11.011
Gopalan, K., Macdougall, J. D., Roy, A. B., and Murali, A. V., 1990, Sm-Nd evidence for 3.3 Ga old rocks in Rajasthan, northwestern India: Precambrian Research, v. 48, n. 3, p. 287–297, https://doi.org/10.1016/0301-9268(90)90013-G
Gregory, L. C., Meert, J. G., Bingen, B., Pandit, M. K., and Torsvik, T. H., 2009, Paleomagnetism and geochronology of the Malani Igneous Suite, Northwest India: Implications for the configuration of Rodinia and the assembly of Gondwana: Precambrian Research, v. 170, n. 1–2, p. 13–26, https://doi.org/10.1016/j.precamres.2008.11.004
Griffin, W. L., Pearson, N. J., Belousova, E., Jackson, S. E., Van Achterbergh, E., O'Reilly, S. Y., and Shee, S. R., 2000, The Hf isotope composition of cratonic mantle: LAM-MC-ICPMS analysis of zircon

megacrysts in kimberlites: Geochimica et Cosmochimica Acta, v. 64, n. 1, p. 133–148, https://doi.org/10.1016/S0016-7037(99)00343-9
Hall, S. M., and Veizer, J., 1996, Geochemistry of Precambrian carbonates: VII. Belt supergroup, Montana and Idaho, USA: Geochimica et Cosmochimica Acta, v. 60, p. 667–677, https://doi.org/10.1016/0016-7037(95)00424-6
Hawkesworth, C., and Kemp, A. I. S., 2006, Using hafnium and oxygen isotopes in zircons to unravel the record of crustal evolution: Chemical Geology, v. 226, n. 3–4, p. 144–162, https://doi.org/10.1016/j.chemgeo.2005.09.018
Hawkesworth, C., Cawood, P., Kemp, T., Storey, C., and Dhuime, B., 2009, Geochemistry: A matter of preservation: Science, v. 323, n. 5910, p. 49–50, https://doi.org/10.1126/science.1168549
Hawkesworth, C. J., Dhuime, B., Pietranik, A. B., Cawood, P. A., Kemp, A. I. S., and Storey, C. D., 2010, The generation and evolution of the continental crust: Journal of the Geological Society, v. 167, n. 2, p. 229, https://doi.org/10.1144/0016-76492009-072
Hawkesworth, C. J., Cawood, P. A., Dhuime, B., and Kemp, T. I. S., 2017, Earth's Continental Lithosphere Through Time: Annual Review of Earth and Planetary Sciences, v. 45, p. 169–198, https://doi.org/10.1146/annurev-earth-063016-020525
Heron, A. M., 1953, Geology of Central Rajputana: Memoir Geological Survey of India, v. 79, 339 p.
Hoskin, P. W. O., and Ireland, T. R., 2000, Rare earth element chemistry of zircon and its use as a provenance indicator: Geology, v. 28, n. 7, p. 627–630, https://doi.org/10.1130/0091-7613(2000)28<627:REECOZ>2.0.CO;2
Hoskin, P. W. O., and Schaltegger, U., 2003, The composition of zircon and igneous and metamorphic petrogenesis: Reviews in Mineralogy and Geochemistry, v. 53, p. 27–62, https://doi.org/10.2113/0530027
Iizuka, T., Komiya, T., Johnson, S. P., Kon, Y., Maruyama, S., and Hirata, T., 2009, Reworking of Hadean crust in the Acasta gneisses, northwestern Canada: Evidence from *in-situ* Lu–Hf isotope analysis of zircon: Chemical Geology, v. 259, n. 3–4, p. 230–239, https://doi.org/10.1016/j.chemgeo.2008.11.007
Iizuka, T., Komiya, T., Rino, S., Maruyama, S., and Hirata, T., 2010, Detrital zircon evidence for Hf isotopic evolution of granitoid crust and continental growth: Geochimica et Cosmochimica Acta, v. 74, n. 8, p. 2450–2472, https://doi.org/10.1016/j.gca.2010.01.023
Iizuka, T., Campbell, I. H., Allen, C. M., Gill, J. B., Maruyama, S., and Makoka, F., 2013, Evolution of the African continental crust as recorded by U–Pb, Lu–Hf and O isotopes in detrital zircons from modern rivers: Geochimica et Cosmochimica Acta, v. 107, p. 96–120, https://doi.org/10.1016/j.gca.2012.12.028
Jackson, S., Pearson, N. J., Griffin, W. L., and Belousova, E. A., 2004, The application of laser ablation-inductively coupled plasma-mass spectrometry to *in situ* U-Pb zircon geochronology: Chemical Geology, v. 211, n. 1–2, p. 47–69, https://doi.org/10.1016/j.chemgeo.2004.06.017
Jan, M. Q., Laghari, A., Khan, M. A., Agheem, M. H., and Khan, T., 2018, Petrology of calc-alkaline/adakitic basement hosting A-type Neoproterozoic granites of the Malani igneous suite in Nagar Parkar, SE Sindh, Pakistan: Arabian Journal of Geosciences, v. 11, p. 25, https://doi.org/10.1007/s12517-017-3378-1
Just, J., Schulz, B., de Wall, H., Jourdan, F., and Pandit, M. K., 2011, Monazite CHIME/EPMA dating of Erinpura granitoid deformation: Implications for Neoproterozoic tectono-thermal evolution of NW India: Gondwana Research, v. 19, n. 2, p. 402–412, https://doi.org/10.1016/j.gr.2010.08.002
Kaur, P., Zeh, A., and Chaudhri, N., 2017b, Palaeoproterozoic continental arc magmatism, and Neoproterozoic metamorphism in the Aravalli-Delhi orogenic belt, NW India: New constraints from *in situ* zircon U-Pb-Hf isotope systematics, monazite dating and whole-rock geochemistry: Journal of Asian Earth Sciences, v. 136, p. 68–88, https://doi.org/10.1016/j.jseaes.2017.01.024
Kaur, P., Chaudhri, N., Raczek, I., Kröner, A., and Hofmann, A. W., 2009, Record of 1.82 Ga Andean-type continental arc magmatism in NE Rajasthan, India: Insights from zircon and Sm–Nd ages, combined with Nd–Sr isotope geochemistry: Gondwana Research, v. 16, n. 1, p. 56–71, https://doi.org/10.1016/j.gr.2009.03.009
Kaur, P., Zeh, A., Chaudhri, N., Gerdes, A., and Okrusch, M., 2011, Archaean to Palaeoproterozoic crustal evolution of the Aravalli mountain range, NW India, and its hinterland: The U–Pb and Hf isotope record of detrital zircon: Precambrian Research, v. 187, n. 1–2, p. 155–164, https://doi.org/10.1016/j.precamres.2011.03.005
Kaur, P., Zeh, A., Chaudhri, N., Gerdes, A., and Okrusch, M., 2013, Nature of magmatism and sedimentation at a Columbia active margin: Insights from combined U–Pb and Lu–Hf isotope data of detrital zircons from NW India: Gondwana Research, v. 23, n. 3, p. 1040–1052, https://doi.org/10.1016/j.gr.2012.07.008
Kaur, P., Zeh, A., Okrusch, M., Chaudhri, N., Gerdes, A., and Brätz, H., 2016, Separating regional metamorphic and metasomatic assemblages and events in the northern Khetri complex, NW India: Evidence from mineralogy, whole-rock geochemistry and U-Pb monazite chronology: Journal of Asian Earth Sciences, v. 129, p. 117–141, https://doi.org/10.1016/j.jseaes.2016.08.002
Kaur, P., Zeh, A., Chaudhri, N., Eliyas, N., 2017a, Two distinct sources of 1.73–1.70 Ga A-type granites from the northern Aravalli orogen, NW India: Constraints from *in situ* zircon U-Pb ages and Lu-Hf isotopes: Gondwana Research, v. 49, p. 164–181, https://doi.org/10.1016/j.gr.2017.05.012
Kemp, A. I. S., Hawkesworth, C. J., Paterson, B. A., and Kinny, P. D., 2006, Episodic growth of the Gondwana supercontinent from hafnium and oxygen isotopes in zircon: Nature, v. 439, p. 580–583, https://doi.org/10.1038/nature04505
Kemp, A. I. S., Hawkesworth, C. J., Collins, W. J., Gray, C. M., Blevin, P. L., and EIMF, , 2009a, Isotopic evidence for rapid continental growth in an extensional accretionary orogen: The Tasmanides, eastern Australia: Earth and Planetary Science Letters, v. 284, n. 3–4, p. 455–466, https://doi.org/10.1016/j.epsl.2009.05.011
Kemp, A. I. S., Foster, G. L., Scherstén, A., Whitehouse, M. J., Darling, J., and Storey, C., 2009b, Concurrent

Pb–Hf isotope analysis of zircon by laser ablation multi-collector ICP-MS, with implications for the crustal evolution of Greenland and the Himalayas: Chemical Geology, v. 261, n. 3–4, p. 244–260, https://doi.org/10.1016/j.chemgeo.2008.06.019

Li, X. H., Long, W. G., Li, Q. L., Liu, Y., Zheng, Y. F., Yang, Y. H., Chamberlain, K. R., Wan, D. F., Guo, C. H., Wang, X. C., and Tao, H., 2010, Penglai Zircon Megacrysts: A Potential New Working Reference Material for Microbeam Determination of Hf–O Isotopes and U–Pb Age: Geostandards and Geoanalytical Research, v. 34, n. 2, p. 117–134, https://doi.org/10.1111/j.1751-908X.2010.00036.x

Li, X. H., Tang, G. Q., Gong, B., Yang, Y. H., Hou, K. J., Hu, Z. C., Li, Q. L., Liu, Y., and Li, W. X., 2013, Qinghu zircon: A working reference for microbeam analysis of U-Pb age and Hf and O isotopes: Chinese Science Bulletin, v. 58, n. 36, p. 4647–4654, https://doi.org/10.1007/s11434-013-5932-x

Li, Z. X., Bogdanova, S. V., Collins, A. S., Davidson, A., De Waele, B., Ernst, R. E., Fitzsimons, I. C. W., Fuck, R. A., Gladkochub, D. P., Jacobs, J., Karlstrom, K. E., Lu, S., Natapov, L. M., Pease, V., Pisarevsky, S. A., Thrane, K., and Vernikovsky, V., 2008, Assembly, configuration, and break-up history of Rodinia: A synthesis: Precambrian Research, v. 160, n. 1–2, p. 179–210, https://doi.org/10.1016/j.precamres.2007.04.021

Liu, Y., Hu, Z., Zong, K., Gao, C., Gao, S., Xu, J., and Chen, H., 2010a, Reappraisement and refinement of zircon U-Pb isotope and trace element analyses by LA-ICP-MS: Chinese Science Bulletin, v. 55, n. 15, p. 1535–1546, https://doi.org/10.1007/s11434-010-3052-4

Liu, Y. S., Gao, S., Hu, Z. C., Gao, C., Zong, K., and Wang, D., 2010b, Continental and Oceanic Crust Recycling-induced Melt-Peridotite Interactions in the Trans-North China Orogen: U-Pb Dating, Hf Isotopes and Trace Elements in Zircons from Mantle Xenoliths: Journal of Petrology, v. 51, n. 1–2, p. 537–571, https://doi.org/10.1093/petrology/egp082

Ludwig, K. R., 2003, User's Manual for Isoplot 3.00, a geolocronolgical Toolkit for Microsoft Excel: Berkeley, California, Berkeley Geochronlogical Center Special Publication, v. 4, p. 25–32.

McKenzie, N. R., Hughes, N. C., Myrow, P. M., Banerjee, D. M., Deb, M., and Planavsky, N. J., 2013, New age constraints for the Proterozoic Aravalli–Delhi successions of India and their implications: Precambrian Research, v. 238, p. 120–128, https://doi.org/10.1016/j.precamres.2013.10.006

Meert, J. G., and Pandit, M. K., 2015, The Archaean and Proterozoic history of Peninsular India: Tectonic framework for Precambrian sedimentary basins in India: Geological Society, London, Memoirs, v. 43, p. 29–54, https://doi.org/10.1144/M43.3

Meert, J. G., Pandit, M. K., and Kamenov, G. D., 2013, Further geochronological and paleomagnetic constraints on Malani (and pre-Malani) magmatism in NW India: Tectonophysics, v. 608, p. 1254–1267, https://doi.org/10.1016/j.tecto.2013.06.019

Merdith, A. S., Collins, A. S., Williams, S. E., Pisarevsky, S., Foden, J. F., Archibald, D. B., Blades, M. L., Alessio, B. L., Armistead, S., Plavsa, D., Clark, C., and Müller, R. D., 2017, A full-plate global reconstruction of the Neoproterozoic: Gondwana Research, v. 50, p. 84–134, https://doi.org/10.1016/j.gr.2017.04.001

Mukhopadhyay, D., Bhattacharyya, T., Chattopadhyay, N., Lopez, R., and Tobisch, O. T., 2000, Anasagar gneiss: A folded granitoid pluton in the Proterozoic South Delhi Fold Belt, central Rajasthan: Proceedings of the Indian Academy of Sciences, Proceedings-Earth and Planetary Sciences, v. 109, n. 1, p. 21–37, https://www.ias.ac.in/article/fulltext/jess/109/01/0022-0038

Nance, R. D., Murphy, J. B., and Santosh, M., 2014, The supercontinent cycle: A retrospective essay: Gondwana Research, v. 25, n. 1, p. 4–29, https://doi.org/10.1016/j.gr.2012.12.026

O'Reilly, S. Y., Griffin, W. L., Pearson, N. J., Jackson, S. E., Belousova, E. A., Alard, O., and Saeed, A., 2008, Taking the pulse of the Earth: Linking crustal and mantle events: Australian Journal of Earth Sciences, v. 55, p. 983–995, https://doi.org/10.1080/08120090802097450

Ozha, M. K., Mishra, B., Hazarika, P., Jeyagopal, A. V., and Yadav, G. S., 2016, EPMA monazite geochronology of the basement and supracrustal rocks within the Pur-Banera basin, Rajasthan: Evidence of Columbia breakup in Northwestern India: Journal of Asian Earth Sciences, v. 117, p. 284–303, https://doi.org/10.1016/j.jseaes.2015.12.016

Pandit, M. K., Sial, A. N., Jamrani, S. S., and Ferreira, V. P., 2001, Carbon isotopic profile across the Bilara Group rocks of Trans-Aravalli Marwar Supergroup in western India: Implications for Meoproterozoic - Cambrian transition: Gondwana Research, v. 4, n. 3, p. 387–394, https://doi.org/10.1016/S1342-937X(05)70338-5

Pandit, M. K., Carter, L. M., Ashwal, L. D., Tucker, R. D., Torsvik, T. H., Jamtveit, B., and Bhushan, S. K., 2003, Age, petrogenesis and significance of 1.0 Ga granitoids and related rocks from the Sendra area, Aravalli Craton, NW India: Journal of Asian Earth Sciences, v. 22, n. 4, p. 363–381, https://doi.org/10.1016/S1367-9120(03)00070-1

Pareek, H. S., 1981, Petrochemistry and Petrogenesis of the Malani Igneous Suite, India: Geological Society of America Bulletin, v. 92, p. 206–273, https://doi.org/10.1130/GSAB-P2-92-206

——— 1984, Pre-Quaternary geology and mineral resources of northwestern Rajasthan: Memoirs of the Geological Survey India, v. 115, p. 1–99.

Patchett, P. J., and Tatsumoto, M., 1981, A routine high-precision method for Lu-Hf isotope geochemistry and chronology: Contributions to Mineralogy and Petrology, v. 75, n. 3, p. 263–267, https://doi.org/10.1007/BF01166766

Pehrsson, S. J., Berman, R. G., Eglington, B., and Rainbird, R., 2013, Two Neoarchean supercontinents revisited: The case for a Rae family of cratons: Precambrian Research, v. 232, p. 27–43, https://doi.org/10.1016/j.precamres.2013.02.005

Pradhan, V. R., Meert, J. G., Pandit, M. K., Kamenov, G., Gregory, L. C., and Malone, S. J., 2010, India's changing place in global Proterozoic reconstructions: A review of geochronologic constraints and paleomagnetic poles from the Dharwar, Bundelkhand and Marwar cratons: Journal of Geodynamics, v. 50, n. 3–4, p. 224–242, https://doi.org/10.1016/j.jog.2009.11.008

Rahaman, M. S., and Mondal, M. E. A., 2015, Evolution of continental crust of the Aravalli craton, NW India, during the Neoarchaean–Palaeoproterozoic: Evidence from geochemistry of granitoids: International Geology Review, v. 57, n. 11–12, p. 1510–1525, https://doi.org/10.1080/00206814.2014.950607

Rathore, S. S., Venkatesan, T. R., and Srivastava, R. K., 1999, Rb-Sr Isotope Dating of Neoproterozoic (Malani Group) Magmatism from Southwest Rajasthan, India: Evidence of Younger Pan-African Thermal Event by ^{40}Ar-^{39}Ar Studies: Gondwana Research, v. 2, n. 2, p. 271–281, https://doi.org/10.1016/S1342-937X(05)70151-9

Rino, S., Komiya, T., Windley, B. F., Katayama, I., Motoki, A., and Hirata, T., 2004, Major episodic increases of continental crustal growth determined from zircon ages of river sands; implications for mantle overturns in the Early Precambrian: Physics of The Earth and Planetary Interiors, v. 146, n. 1–2, p. 369–394, https://doi.org/10.1016/j.pepi.2003.09.024

Roberts, N. M. W., 2012, Increased loss of continental crust during supercontinent amalgamation: Gondwana Research, v. 21, n. 4, p. 994–1000, https://doi.org/10.1016/j.gr.2011.08.001

Roberts, N. M. W., and Slagstad, T., 2015, Continental growth and reworking on the edge of the Columbia and Rodinia supercontinents; 1.86–0.9 Ga accretionary orogeny in southwest Fennoscandia: International Geology Review, v. 57, n. 11–12, p. 1582–1606, https://doi.org/10.1080/00206814.2014.958579

Rogers, J. J. W., and Santosh, M., 2003, Supercontinents in Earth History: Gondwana Research, v. 6, n. 3, p. 357–368, https://doi.org/10.1016/S1342-937X(05)70993-X

Roy, A. B., and Jakhar, S. R., 2002, Geology of Rajasthan: Precambrian to Recent: Jodhpur, India, Scientific Publishers, 421 p.

Roy, A. B., and Kröner, A., 1996, Single zircon evaporation ages constraining the growth of the Archaean Aravalli craton, northwestern Indian shield: Geological Magazine, v. 133, n. 3, p. 333–342, https://doi.org/10.1017/S0016756800009067

Singh, Y. K., De Waele, B., Karmakar, S., Sarkar, S., and Biswal, T. K., 2010, Tectonic setting of the Balaram-Kui-Surpagla-Kengora granulites of the South Delhi Terrane of the Aravalli Mobile Belt, NW India and its implication on correlation with the East African Orogen in the Gondwana assembly: Precambrian Research, v. 183, n. 4, p. 669–688, https://doi.org/10.1016/j.precamres.2010.08.005

Sinha Roy, S., Malhotra, G., and Mohanty, M. K., 1998, Geology of Rajasthan: Bangalore, India, Geological Society of India, 278 p.

Solanki, A. M., ms, 2011, A petrographic, geochemical and geochronological investigation of deformed granitoids from SW Rajasthan: Neoproterozoic age of formation and evidence of Pan-African imprint: Johannesburg, South Africa, University of the Witwatersrand Johannesburg, M. Sc. Thesis, 216 p.

Spencer, C. J., Hawkesworth, C., Cawood, P. A., and Dhuime, B., 2013, Not all supercontinents are created equal: Gondwana-Rodinia case study: Geology, v. 41, n. 7, p. 795–798, https://doi.org/10.1130/G34520.1

Spencer, C. J., Roberts, N. M. W., and Santosh, M., 2017, Growth, destruction, and preservation of Earth's continental crust: Earth-Science Reviews, v. 172, p. 87–106, https://doi.org/10.1016/j.earscirev.2017.07.013

Stein, M., and Hofmann, A. W., 1994, Mantle plumes and episodic crustal growth: Nature, v. 372, p. 63–68, https://doi.org/10.1038/372063a0

Thirlwall, M. F., and Anczkiewicz, R., 2004, Multidynamic isotope ratio analysis using MC–ICP–MS and the causes of secular drift in Hf, Nd and Pb isotope ratios: International Journal of Mass Spectrometry, v. 235, n. 1, p. 59–81, https://doi.org/10.1016/j.ijms.2004.04.002

Torsvik, T. H., Ashwal, L. D., Tucker, R. D., and Eide, E. A., 2001a, Neoproterozoic geochronology and palaeogeography of the Seychelles microcontinent: The India link: Precambrian Research, v. 110, n. 1–4, p. 47–59, https://doi.org/10.1016/S0301-9268(01)00180-2

Torsvik, T. H., Carter, L. M., Ashwal, L. D., Bhushan, S. K., Pandit, M. K., and Jamtveit, B., 2001b, Rodinia refined or obscured: Palaeomagnetism of the Malani igneous suite (NW India): Precambrian Research, v. 108, n. 3–4, p. 319–333, https://doi.org/10.1016/S0301-9268(01)00139-5

Valley, J. W., Lackey, J. S., Cavosie, A. J., Clechenko, C. C., Spicuzza, M. J., Basei, M. A. S., Bindeman, I. N., Ferreira, V. P., Sial, A. N., King, E. M., Peck, W. H., Sinha, A. K., and Wei, C. S., 2005, 4.4 billion years of crustal maturation: Oxygen isotope ratios of magmatic zircon: Contributions to Mineralogy and Petrology, v. 150, n. 6, p. 561–580, https://doi.org/10.1007/s00410-005-0025-8

Van Lente, B., Ashwal, L. D., Pandit, M. K., Bowring, S. A., and Torsvik, T. H., 2009, Neoproterozoic hydrothermally altered basaltic rocks from Rajasthan, northwest India: Implications for late Precambrian tectonic evolution of the Aravalli Craton: Precambrian Research, v. 170, n. 3–4, p. 202–222, https://doi.org/10.1016/j.precamres.2009.01.007

Vervoort, J. D., and Kemp, A. I. S., 2016, Clarifying the zircon Hf isotope record of crust–mantle evolution: Chemical Geology, v. 425, p. 65–75, https://doi.org/10.1016/j.chemgeo.2016.01.023

Vervoort, J. D., and Patchett, P. J., 1996, Behavior of hafnium and neodymium isotopes in the crust: Constraints from Precambrian crustally derived granites: Geochimica et Cosmochimica Acta, v. 60, n. 19, p. 3717–3733, https://doi.org/10.1016/0016-7037(96)00201-3

Voice, P. J., Kowalewski, M., and Eriksson, K. A., 2011, Quantifying the Timing and Rate of Crustal Evolution: Global Compilation of Radiometrically Dated Detrital Zircon Grains: The Journal of Geology, v. 119, n. 2, p. 109–126, https://doi.org/10.1086/658295

Wan, Y., Ma, M., Dong, C., Xie, H., Xie, S., Ren, P., and Liu, D., 2015, Widespread late Neoarchean reworking of Meso- to Paleoarchean continental crust in the Anshan-Benxi area, North China Craton, as documented by U-Pb-Nd-Hf-O isotopes: American Journal of Science, v. 315, n. 7, p. 620–670, https://doi.org/10.2475/07.2015.02

Wang, C. Y., Campbell, I. H., Allen, C. M., Williams, I. S., and Eggins, S. M., 2009, Rate of growth of the preserved North American continental crust: Evidence from Hf and O isotopes in Mississippi detrital

zircons: Geochimica et Cosmochimica Acta, v. 73, n. 3, p. 712–728, https://doi.org/10.1016/j.gca.2008.10.037

Wang, C. Y., Campbell, I. H., Stepanov, A. S., Allen, C. M., and Burtsev, I. N., 2011, Growth rate of the preserved continental crust: II. Constraints from Hf and O isotopes in detrital zircons from Greater Russian Rivers: Geochimica et Cosmochimica Acta, v. 75, n. 5, p. 1308–1345, https://doi.org/10.1016/j.gca.2010.12.010

Wang, W., Zhou, M. F., Yan, D. P., Li, L., and Malpas, J., 2013, Detrital zircon record of Neoproterozoic active-margin sedimentation in the eastern Jiangnan Orogen, South China: Precambrian Research, v. 235, p. 1–19, https://doi.org/10.1016/j.precamres.2013.05.013

Wang, W., Cawood, P. A., Pandit, M. K., Zhou, M. F., and Chen, W. T., 2017a, Zircon U-Pb age and Hf isotope evidence for Eoarchean crustal remnant and episodic crustal growth and reworking in response to supercontinental cycles in NW India: Journal of the Geological Society, v. 174, n. 4, p. 759–772, https://doi.org/10.1144/jgs2016-080

Wang, W., Cawood, P. A., Zhou, M. F., Pandit, M. K., Xia, X. P., and Zhao, J. H., 2017b, Low-$\delta^{18}O$ rhyolites from the Malani Igneous Suite: A positive test for South China and NW India linkage in Rodinia: Geophysical Research Letters, v. 44, n. 20, p. 10298–10305, https://doi.org/10.1002/2017GL074717

Wang, W., Pandit, M. K., Zhao, J. H., Chen, W. T., and Zheng, J. P., 2018, Slab break-off triggered lithosphere - asthenosphere interaction at a convergent margin: The Neoproterozoic bimodal magmatism in NW India: Lithos, v. 296–299, p. 281–296, https://doi.org/10.1016/j.lithos.2017.11.010

Wang, W., Cawood, P. A., Pandit, M. K., Zhou, M. F., and Zhao, J. H., 2019, Evolving passive and active margin tectonics of the Paleoproterozoic Aravalli Supergroup, NW India: Geological Society of America Bulletin, https://doi.org/10.1130/B35027.1

Wiedenbeck, M., and Goswami, J. N., 1994, High precision $^{207}Pb/^{206}Pb$ zircon geochronology using a small ion microprobe: Geochimica et Cosmochimica Acta, v. 58, n. 9, p. 2135–2141, https://doi.org/10.1016/0016-7037(94)90291-7

Wiedenbeck, M., Allé, P., Corfu, F., Griffin, W. L., Meier, M., Oberli, F., von Quadt, A., Roddick, J. C., and Spiegel, W., 1995, Three natural zircon standards for U-Th-Pb, Lu-Hf, Trace element and REE analyses: Geostandards and Geoanalytical Research, v. 19, n. 1, p. 1–23, https://doi.org/10.1111/j.1751-908X.1995.tb00147.x

Wiedenbeck, M., Goswami, J. N., and Roy, A. B., 1996, Stabilization of the Aravalli Craton of northwestern India at 2.5 Ga: An ion microprobe zircon study: Chemical Geology, v. 129, n. 3–4, p. 325–340, https://doi.org/10.1016/0009-2541(95)00182-4

Wu, F. Y., Yang, Y. H., Xie, L. W., Yang, J. H., and Xu, P., 2006, Hf isotopic compositions of the standard zircons and baddeleyites used in U-Pb geochronology: Chemical Geology, v. 234, n. 1–2, p. 105–126, https://doi.org/10.1016/j.chemgeo.2006.05.003

Wu, Y. B., and Zheng, Y. F, 2004, Genesis of zircon and its constraints on interpretation of U-Pb age: Science Bulletin, v. 49, n. 15, p. 1554–1569, https://doi.org/10.1007/BF03184122

Yang, Q., Xia, X. P., Zhang, W. F., Zhang, Y. Q., Xiong, B. Q., Xu, Y. G., Wang, Q., and Wei, G. J., 2018, An evaluation of precision and accuracy of SIMS oxygen isotope analysis: Solid Earth Sciences, v. 3, n. 3, https://doi.org/10.1016/j.sesci.2018.05.001

Yuan, H. L., Gao, S., Dai, M. N., Zong, C. L., Gunther, D., Fontaine, G. H., Liu, X. M., and Diwu, C. R., 2008, Simultaneous determinations of U-Pb age, Hf isotopes and trace element compositions of zircon by excimer laser-ablation quadrupole and multiple-collector ICP-MS: Chemical Geology, v. 247, n. 1–2, p. 100–118, https://doi.org/10.1016/j.chemgeo.2007.10.003

Zhao, J. H., Pandit, M. K., Wang, W., and Xia, X. P., 2018, Neoproterozoic tectonothermal evolution of NW India: Evidence from geochemistry and geochronology of granitoids: Lithos, v. 316–317, p. 330–346, https://doi.org/10.1016/j.lithos.2018.07.020